Climate Change Initiative+ (CCI+) Phase 2

Sea Surface Salinity

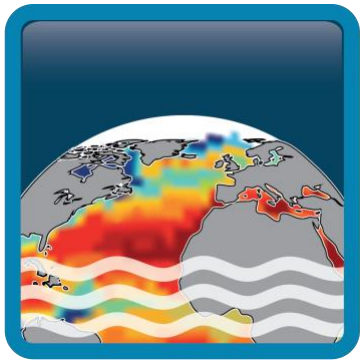

[D5.1]Climate Assessment Report (CAR)

Customer: ESA

Ref.: ESA-EOP-SC-AMT-2021-26

Version: v4.0

Ref. internal: 4000123663/18/I-NB

Revision Date: 29/11/2023

Filename: SSS_cci_PHASE#02_D5.1_CAR_v4r1.docx

Deliverable code: D5.1

Signatures

Author	Manon Gévaudan, Julien Jouanno, Nicolas Kolodziejczyk, Matthew Martin, Elisabeth Remy,Roshin Raj, Gilles Reverdin	LEGOS, LEGOS, MOI, LOCEAN, MetOffice, LOPS, NERSC, LOCEAN	
Reviewed By			
Approved By	Jacqueline Boutin (Science Leader)	LOCEAN	
	Nicolas Reul (Science Leader)	IFREMER	
	Rafael Catany (Project Manager)	ARGANS	
	Roberto Sabia (Technical Officer)	ESA	
Accepted By	Roberto Sabia (Technical Officer)	ESA	

Diffusion List
Sea Surface Salinity Team Members
ESA (Roberto Sabia, Susanne Mecklenburg)

Amendment Record Sheet

Date / Issue	Description	Section / Page
29/10/2023 / v4.0	Issue document to ESA	NA

Table of Contents

List of figures

List of tables

Acronyms

AMM	Atlantic Meridional Mode
AMOC	Atlantic Meridional Overturning Circulation
CATDS	Centre Aval de Traitement des Données SMOS
CCI	Climate Change Initiative
EAP	East Atlantic Pattern
ECV	Essential Climate Variable
ENKF	ensemble Kalman filter method
ENSO	El Nino Southern Oscillation
FOAM	Forecasting Ocean Assimilation Model
FWC	Fresh Water Content
HYCOM	HYbrid Coordinate Ocean Model
ITCZ	Inter Tropical Convergence Zone
NAO	North Atlantic Oscillation
NBC	North Brazil Current
NEMO	Nucleus for European Modelling of the Ocean
PISCES	Pelagic Interactions Scheme for Carbon and Ecosystem Studies
RMSD	Root Mean Square difference
SCAN	Scandinavian Pattern
SMOS	Soil Moisture and Ocean Salinity mission
SPCZ	South Pacific Convergence zone
SSS	Sea surface salinity
SST	Sea Surface Temperature
TDOM	Terrestrial Dissolved Organic Matter
WRF	Weather Research and Forecasting model

1 Introduction

1.1 Scope of this document

The Climate Change Initiative (CCI) is a program of the European Space Agency aiming to build the longest time series of the Essential Climate Variable (ECV) Sea Surface Salinity (SSS).

This document presents a climate assessment of the European Space Agency Sea Surface Salinity Climate Change Initiative (ESA CCI+SSS) Phase 2 products (version 3 and version4). The document describes the results of the usage and application of the CCI+SSS project sea surface salinity data sets in climate research and for inter-comparison to model data and for usage in assimilation experiments.

1.2 Structure of the document

This document is structured as follows:

Chapter 1 Introduction

Chapter 2 described the progress achieved on **Tropical Regional cases studies**

- Influence of the Amazon-Orinoco discharge interannual variability on the western tropical Atlantic salinity and temperature
- Transport of the Amazon discharge in intermittent eddy structures (late summer/fall focus)
- Calibration of Amazon dissolved organic matter optical properties in a biogeochemical model using CCI observations

Chapter 3 described the progress achieved on **Artic regional cases studies**

- Sea Surface Salinity Polar Front variability in Barents Sea from in situ and satellite missions
- Impact of freshwater anomalies on Barents Sea dense water formation inferred from model reanalysis
- The role of atmospheric variability on the Barents Sea salinity

Chapter 4 present activities performed by **operational centers**:

- Data assimilation of SSS and impact on an ocean reanalysis
- Characterization of SSS variability and errors in ocean reanalysis
- Chapter 5 provides a summary of the main achievements.

1.3 Satellite products used is the case studies and reference to proposal

Depending on the temporality and availability of data, and the technical or scientific constraints of the various study cases, different products were used. They are listed in the table below.

Study title	SSS product	Primary institute and reference to the proposal
Influence of the Amazon-Orinoco discharge interannual variability on the western tropical Atlantic salinity and temperature	*CCI+SSS V4.4 (and V3)*	LEGOS /Main Proposal – Case study 3 Process of variability of the Amazon plume
Calibration of Amazon dissolved organic matter optical properties in a biogeochemical model using CCI observations.	*CCI+SSS V4.4 (and V3)*	LEGOS - Main Proposal - Case study 3 Process of variability of the Amazon plume
Transport of the Amazon discharge in intermittent eddy structures (late summer/fall focus)	High-resolution SSS product develop (with SMOS and SMAP data). Reason: exponential kernel required to track fast propagating fresh water lenses.	LOCEAN - Main Proposal Case study 3 - Process of variability of the Amazon plume
Sea Surface Salinity Polar Front variability in Barents Sea from in situ and satellite missions	*CCI+SSS V4.4*	LOPS - Option Proposal Case study 1 - Sea Surface Salinity Polar Front variability in Barents Sea from in situ and satellite missions.
Impact of freshwater anomalies on Barents Sea dense water formation inferred from model reanalysis	*CCI+SSS V4.4*	NERSC - Option Proposal Case study 2 - The role of atmospheric variability on the Barents Sea salinity
The role of atmospheric variability on the Barents Sea salinity	*CCI+SSS V4.4*	NERSC - Option Proposal Case study 2 - The role of atmospheric variability on the Barents Sea salinity
Data assimilation of SSS and impact on an ocean reanalysis	SMOS and SMAP L2 products (unavailability of CCI+SSS L2 products)	Met Office - Main proposal Case Study 1 - Data Assimilation of SSS and impact on an ocean reanalysis
Characterization of SSS variability and errors in ocean reanalysis	*CCI+SSS V3*	Mercator Ocean International - Main proposal Case study 2 - Interannual variability of the Sea Surface Salinity in the global ocean reanalysis GLORYS12 compared to ESA CCI+ SSS product.

Table 1 Summary of the products used in the case study and link of the case studies with the CCI+SSS proposal.

2 TROPICAL REGIONAL CASE STUDIES

2.1 Influence of the Amazon-Orinoco discharge interannual variability on the western tropical Atlantic salinity and temperature (M. Gévaudan)

Contributors : M. Gévaudan, J. Jouanno, F. Durand

Climate relevance: This case study highlights the interconnectedness of various factors influencing SSS and SST and the role of large-scale climate patterns like the Atlantic meridional mode (AMM) in shaping their interannual dynamics. It emphasizes the influence of runoff interannual variability, particularly from the Amazon River, on SSS changes in the tropical Atlantic, but also underscores the importance of ocean dynamics and atmospheric circulation patterns in shaping SSS variability which contribute to around half of the observed SSS response. The combination between model and CCI+SSS observations over the Amazon plume contributes to a better understanding of regional climate variability.

This case study investigates the impact of Amazon flooding on sea surface salinity (SSS) and sea surface temperature (SST). Indeed, over the last three decades, extreme floods and droughts have become more frequent in the Amazon basin, strongly affecting the population and ecosystems in the region (e.g., Barichivich et al., 2018). However, the impact of these extreme events on the tropical Atlantic Ocean is still poorly understood.

To study this, we developed a 1/4° coupled ocean-atmosphere configuration of the tropical Atlantic Ocean, using NEMO, WRF and OASIS (see Gévaudan et al. 2021 for more details). We first validated the mean state and the interannual variability of SSS in the model by comparing it to CCI observations (Figure 1). The coupled model was run from 2001 to 2015 and can be compared to CCI data from 2010 to 2015 only. To compare to longer time series, we also study the results of a forced ocean model of the region that was run from 2001 to 2022.

The coupled model reproduces very well the mean state in the whole tropical Atlantic basin (Figure 1a,b). The seasonal cycle in the Amazon plume is also very close to the observations, except for a slightly too low SSS during the flood season (Figure 1e). It has a slightly too high standard deviation compared to the satellite observations (Figure 1c,d), but the interannual variability compares well to the observations, apart in 2011 where it is too low (Figure 1f). The forced model is too fresh (Figure 1e), which is probably partly caused by a too weak wind forcing. Yet the interannual variability is similar between the forced and coupled model for most of the time series, apart from 2008 to 2010. We can also notice a higher variability in the forced model at the beginning of the time series. This discrepancy might be due to the different runoff forcings used. From 2012 to 2015, the interannual variability is very well reproduced by both models. From 2016 onwards, the forced model follows the observations but seems to overestimate once again the variability (too strong positive and negative peaks).

Overall, the coupled model compares very well with CCI observations, and would be expected to perform very well until the end of the CCI observational time series.

Using this coupled configuration, two simulations were carried out: one with interannual monthly river flows (called REF), and one with climatological monthly river flows (called CLIM). Some composites of the years with strong floodings and the years with weak floodings were also calculated. By comparing the composites for these two simulations, we can dissociate the

changes in SSS and SST caused by the interannual variability of the rivers from the changes caused by the interannual variability of the ocean and the atmosphere, and quantify them.

Regarding SSS, the results are shown in Figure 2. A strong interannual variability is observed in spring close to the Amazon mouth: the years with strong floodings have a SSS down to 12 PSS lower than the years with weak floodings (Figure 2a). But this effect is limited in time (a few months) and space (a few hundred kilometers): the SSS response is already much weaker in summer (Figure 2b)

This interannual variability is partly caused by the runoff interannual variability (Figure 2c,d). But the variability in ocean dynamics and atmosphere is also important, and accounts for around half of the SSS response (Figure 2e,f). Indeed, the ocean and atmospheric variability induce changes in the currents (see arrows on Figure 2 e,f) that strongly impact the SSS. In spring, a weakening of the North Brazil Current is observed, leading to an accumulation of freshwater near the Amazon mouth (negative anomaly), and less northwestward offshore export of freshwater (positive anomaly. In summer, a strengthening of the North Brazil Current induces more freshwater export in the Lesser Antilles and therefore a negative anomaly. At the same time, a weakening of the North Equatorial Counter Current induces less eastward freshwater transport, leading to a positive anomaly east of the plume.

As done for the SSS, we isolate the effect of the runoff interannual variability on the SST (Figure 3a,b) from the changes due to the ocean dynamics and atmosphere (Figure 3,d). The results show that years of strong floodings and weak floodings generally coincide with abnormal phases of one of the Atlantic's variability modes, the Atlantic meridional mode (AMM). Indeed, the AMM is associated with large-scale SST anomalies in the tropical Atlantic Ocean that are very similar to those observed on Figure 3c (e.g., Foltz et al., 2012). The SST anomalies caused by AMM tend to disappear in summer, which is what we can see on Figure 3d. Finally, despite a strong change in SSS (Figure 3c,d), the runoff interannual variability leads to very weak changes in SST in spring and summer (Figure 3a,b).

For more details on this study, you can refer to Gévaudan et al., 2022.

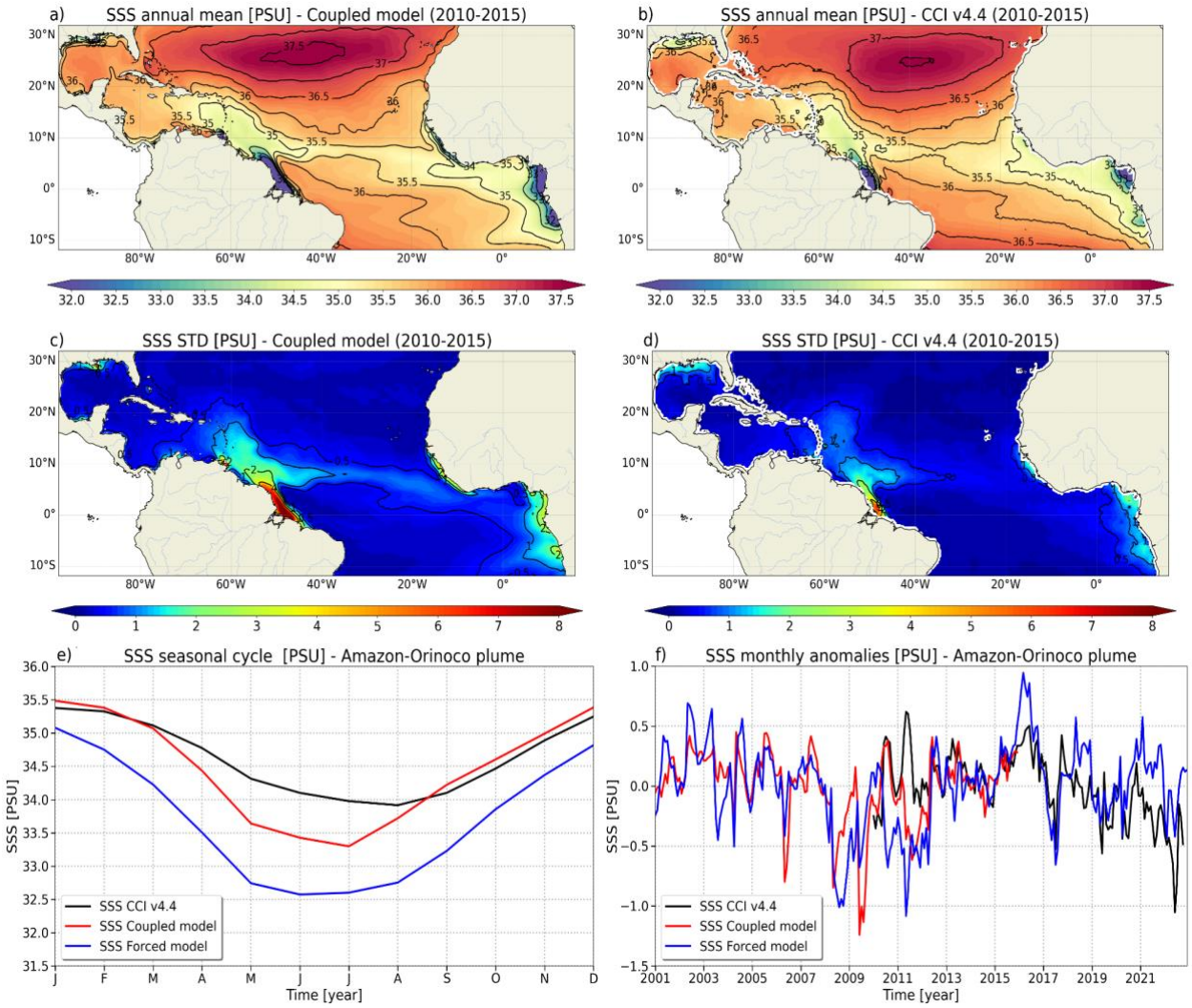

Figure 1 Annual mean SSS for a) the coupled model and b) CCI v4.4 observations. Standard deviation of SSS for c) the coupled model and d) CCI v4.4 observations. e) Seasonal cycle of SSS and f) monthly anomalies of SSS for CCI v4.4 observations (black), the coupled model (red) and the forced model (blue).

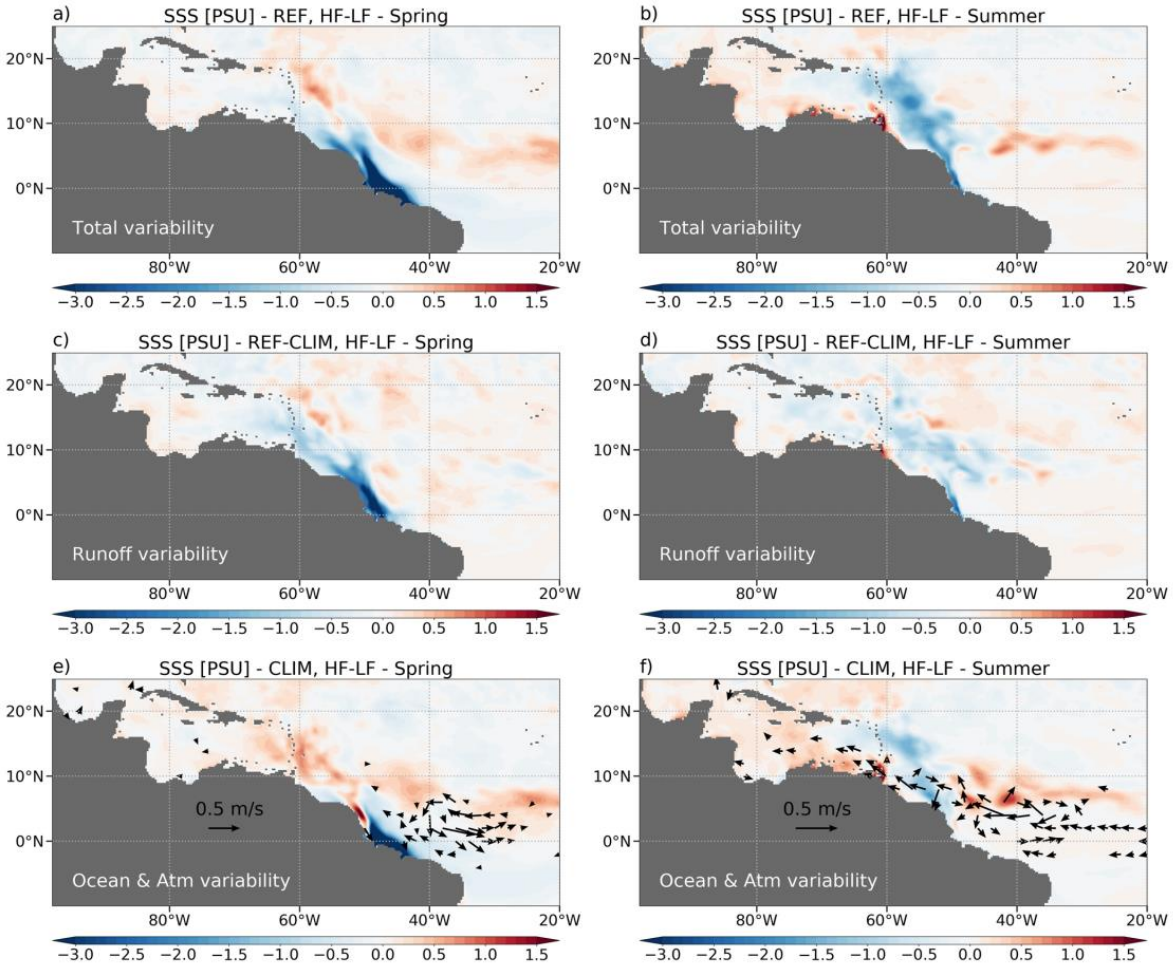

Figure 2 Spring (April-May-June, AMJ) maps of SSS differences between highest floods and lowest floods composites for (a) REF, (c) REF – CLIM and (e) CLIM; (b, d and f): same as (a, c and e) respectively but for the summer season (July-August-September, JAS); the arrows on (e and f) represent the current anomalies with a norm greater than 0.1 m/s

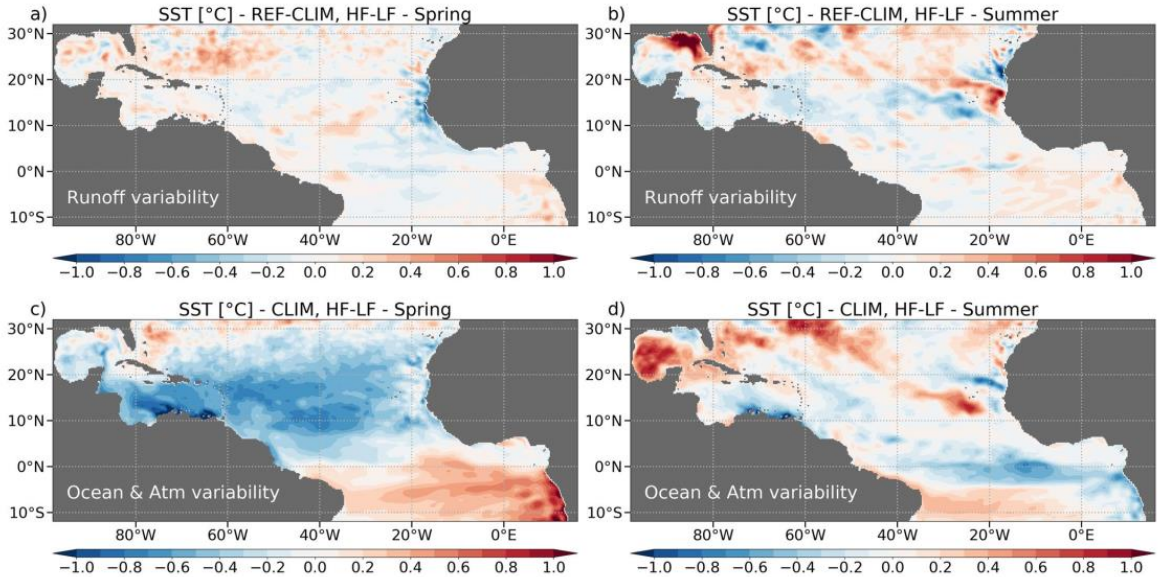

Figure 3 Spring (AMJ) maps of SST differences between highest floods and lowest floods for (a) CLIM and (c) REF – CLIM; (b and d): same as (a and c) respectively but in summer (JAS)

2.2 Transport of the Amazon discharge in intermittent eddy structures (late summer/fall focus) (G. Reverdin)

Contributors: L. Olivier, G. Reverdin, J. Boutin, LOCEAN, J.-L. Vergely, ACRI-ST

Climate relevance of this case study. Remote sensing observations in this case study provide new insights into the pathways and dynamics of freshwater transport from the Amazon River, particularly during late summer and fall. The study emphasizes the need for improved models that can capture the fast-evolving freshwater structures and their interactions with ocean dynamics. Such models would be essential for better understanding and predicting the impacts of Amazon River freshwater transport on regional climate and marine systems.

In late summer/fall, the transport of the freshwater of the Amazon is classically thought to be mostly eastward north of the equator in the North Equatorial Counter Current, feeding the central North tropical Atlantic with its nutrients and CO2-depleted waters. Meanwhile, near the Antilles, the warm pool which is expected to have earlier been fed in fresh and stratified surface waters, can interact with cyclone development due to the enhanced fresh surface water driven/stratification.

The emphasis of this study (Olivier et al., 2023) was two-folds: document the paths of the freshwater transport during that season, and investigate the fresh surface layer thickness from in situ data. It was inspired by data collected in August-September 2023 during the Tara-Microbiome and Amazomix cruises, which documented very rapid changes in the fresher surface water structures, in particular at the time when the freshwater separated from the shelf in early to mid-September. It also identified large transport by meso-scale structures. To capture this fast variability and not overly blur the structures, we have thus used a special high-resolution product develop at CATDS (with SMOS and SMAP data), which relies on an exponential kernel, and not the one distributed as CCI V4.4 which relies a Gaussian kernel in the Bayesian approach. Comparison to in situ data in this region showed that the exponential-kernel performed better to capture these ‘fast’ structures. Nonetheless most of the results we present will also be found but probably less precisely by using the CCI V4.4 product.

We first illustrate the path and evolution of a remarkable freshwater pool in September -October 2021, which was particularly well tracked and studies due to upstream sampling during Tara-Microbiome and Amazomix cruises, was sampled by near surface (drogues either at 50 cm or 15-m) drifters and was sampled at least three times by Argo floats (but not in the initial phase, when it was separating from the shelf, due to difficulties some Argo floats have when near-surface stratification is too strong (Reverdin et al., 2023).

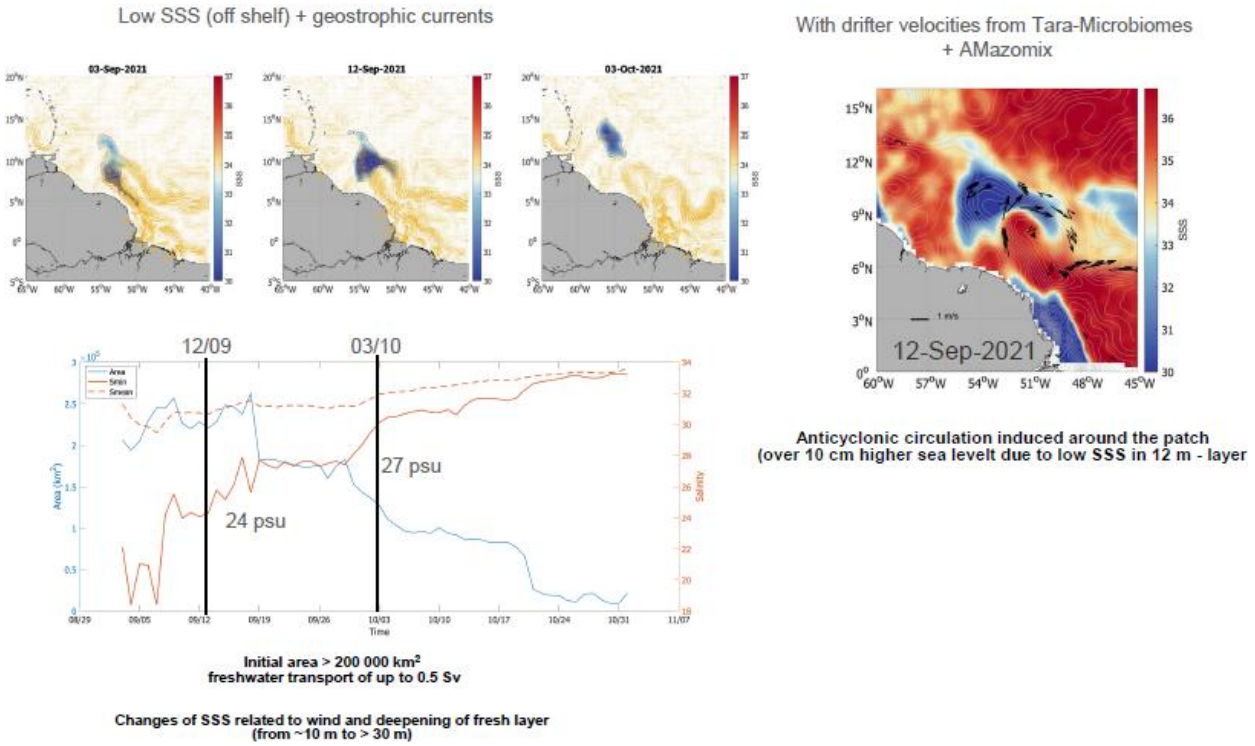

Figure 4. Illustration of the September-formed freshwater pool and evolution. The top panel shows the salinity in that pool (within the 34.5 S contour) at three dates illustrating its separation from the shelf (Sep. 3), its mature phase north of an anti-cyclonic eddy (yellow arrows show geostrophic currents on Sep 12) (an there is a zoom on right panel with drifter velocities on that date and contours of surface elevation), and its following drift northward (October 3). The lower panel presents the time evolution of SSS in its core (orange) as well as area covered (blue).

This fresh structure (Figure 4) is very intense with initial SSS of 24 until September 12, increasing to 27 for close to 10 days. At this time, and Argo profile indicates a 12-m thick fresh surface layer. It is intense enough to contribute to a 10-cm surface elevation that is documented in the altimetric data, and associated with a small anticyclonic structure, northwest of the more intense NBC ring with a salty core. The core salinity increases each time there are strong winds (such as after October 1), at which time the structure drifts northward or northwestward with the Ekman currents, and the fresh layer deepens (to more than 30-m by mid-October).

How common are such intense structures (initially covering 2000 0000 km^2) and transport of low salinity surface water impacted by the Amazon outflow? To answer the question, we estimate freshwater transport across sections, both to the east (towards the North Equatorial Counter Current) and to the northwest (towards the Caribbean), in this case a little northwest of the retroflection. This is done with an assumed fixed layer thickness (based on the few profiles in freshwater pools in this area), the daily SSS product, Aviso geostrophic currents and estimated Ekman currents.

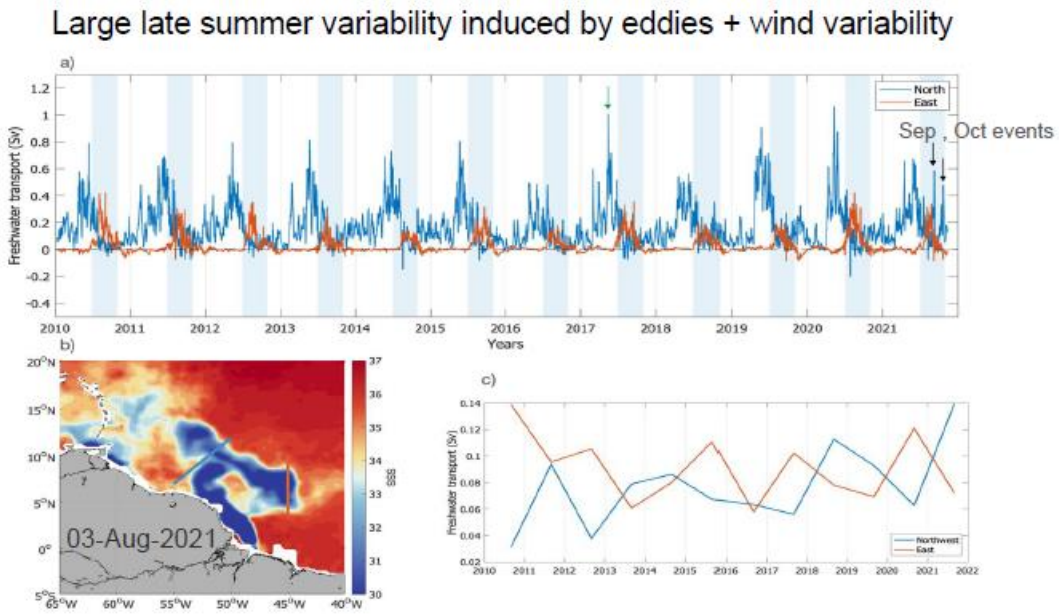

Figure 5 Lower left panel indicates the blue (NW) and red (E) sections across which the freshwater transport is estimated on a daily basis. The top panel shows the two transport time series in 2010-2021, whereas the lower right panel shows interannual time series in 2010-2021, whereas the lower right panel shows interannual time series of August-October average transport (of a smoothed 40-day version of the top curves).

The positions of the sections are shown on the lower panel, at a time when there had been northwestward transport, but associated with strong eastward transport (in a fresh layer shallower than 10-m based on an Argo float). The time series (top panel of Figure 5) illustrate the intermittency of the transports E and NW in all seasons, as well as the presence of transport through E only in the summer-fall season as was expected. For NW during this season, it also shows two very large spikes in Sep. and Oct. 2021 with peak transport of 0.5 Sv, which are well above what happened during other years. When averaging the transports over the season August-October (lower right panel), we found that the NW transport averages over this period nearly as much as the E transport (larger in 2018, 2019 and 2021). The largest transport by far however happened in 2021 and is associated with the two eddy structures. There is obviously a very large interannual variability in these transports and potentially some longer trends, although the time series is of too short duration to illustrate that.

2.3 Calibration of Amazon dissolved organic matter optical properties in a biogeochemical model using CCI observations (M. Gévaudan)

Contributors: M. Gévaudan, J. Jouanno, O. Aumont, J. Boutin

Climate relevance of this study. The cross analysis of CCI SSS and CCI ocean color allows to establishes a link between SSS and Terrestrial Dissolved Organic Matter (TDOM) allowing to calibrate the representation of TDOM in ocean model and its impact on ocean color absorption. This improves the model's ability to capture the spatial and temporal variability of phytoplankton blooms. Improving the representation of phytoplankton blooms in the large river plumes is crucial for assessing their role in the marine carbon cycle and predicting their response to climate change.

The Amazon River discharges large fluxes of nutrients that sustain phytoplanktonic blooms until far offshore (e.g., Dagg et al., 2004). But the exact cause and mechanisms behind these blooms are not yet fully understood. Nitrogen is the main limiting nutrient in the region (e.g., Subramaniam et al., 2008), but what is the main source of nitrogen in the offshore part of the

plume? And does the strong salinity stratification induced by the Amazon plume have a role to play? To answer these questions, a coupled ocean-biogeochemical model is necessary. But models of the region are still not able to reproduce these offshore blooms (e.g., Da Cunha et al., 2013, Louchard et al., 2021). This case study therefore aims to provide a coupled ocean-biogeochemical configuration capable of reproducing these blooms, as a first step towards assessing the impact of SSS and salinity stratification on phytoplanktonic blooms in the region. To this end, we developed a 1/4° NEMO-PISCES configuration of the tropical Atlantic Ocean, and we improved the representation of the terrestrial dissolved organic matter (TDOM) in the biogeochemical model.

TDOM is the dissolved organic matter discharged by the rivers. It has mainly two effects that are missing in PISCES. First, its remineralization rate is lower than that of the dissolved organic matter of the ocean. Second, it has a shading effect that attenuates the penetration of the solar flux into the ocean. To include these two missing mechanisms into the model, we added a TDOM tracer remineralized solely by photodegradation and bacterial degradation. We then calculated the associated absorption coefficient (a_{CDOM}) and added it to the solar penetration scheme of the model.

Obtaining the relationship between TDOM concentration and a_{CDOM} is not straightforward, because there is no observation of TDOM concentration. Therefore, we decided to use SSS as an intermediate. Indeed, the relationship between SSS and a_{CDOM} in the Amazon plume has already been extensively studied, and can be retrieved with satellite data (e.g., Del Vecchio et al, 2004, Fournier et al., 2015). But since SSS data time series are now longer, we decided to update the relationship they found. We use monthly data from CCI Ocean Colour v6.0, and CCI SSS v3.2 (the last version available at the beginning of the study), between January 2010 and September 2020. We first assess the correlation between SSS and a_{CDOM} (Figure 6a). As observed by Fournier et al., 2015, the two variables are strongly anti-correlated in the whole Amazon plume (up to -0.9 near the Amazon mouth). We then remove data that are too weakly correlated: we chose a threshold of R^2=0.6, and plotted the relationship between SSS and a_{CDOM} for the points higher than this threshold ((Figure 6b). We can see that the relationship is best described by an exponential regression, contrary to what was obtained by the previous studies. This is probably due to the fact that the CCI data are able to reach closer to the coast, which allows us to have SSS data close to 0 PSS. This was not the case for the previous studies, which had data down to 22 to 31 PSS only.

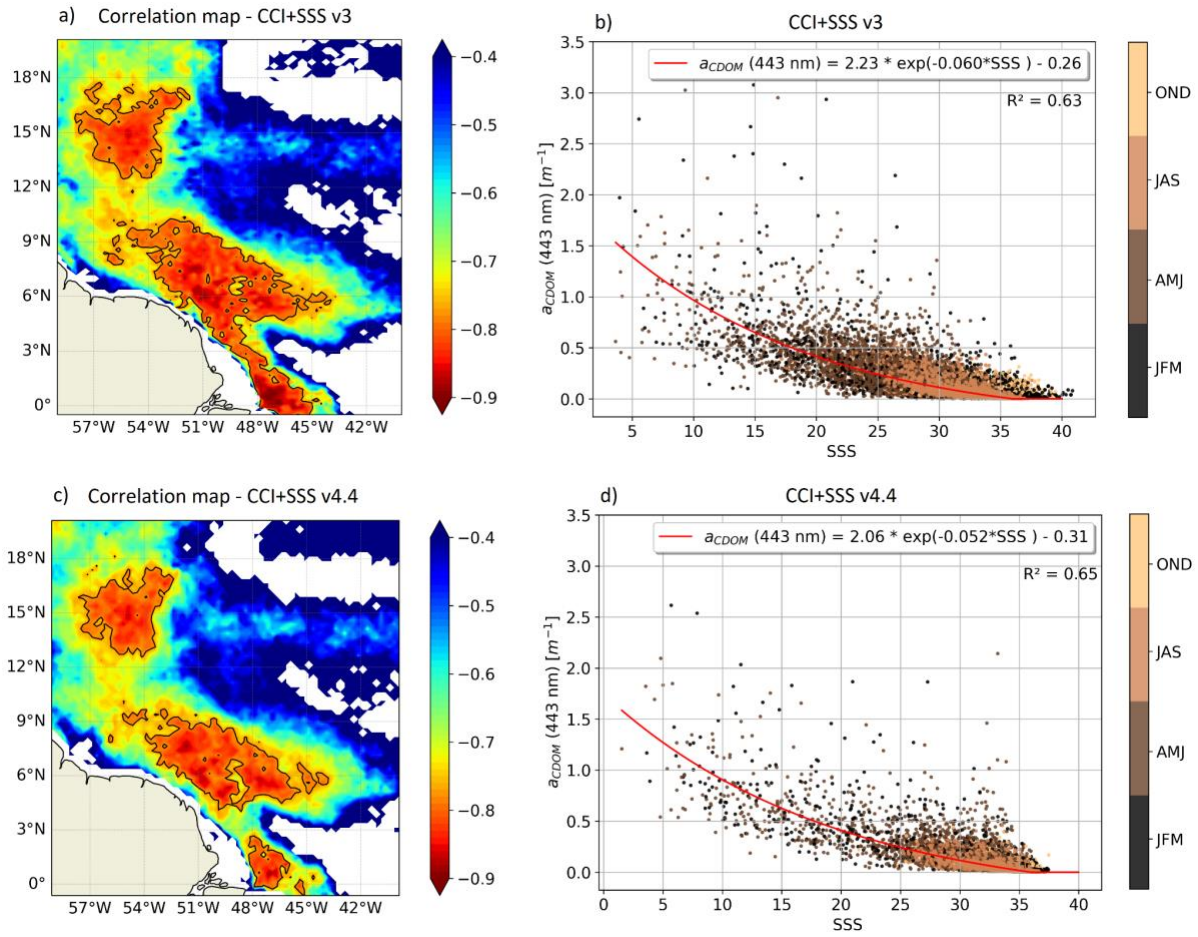

Figure 6 a) Correlation map (R) between SSS and aCDOM in the Amazon plume. The black contour shows the isoline R^2=0.6 ; b) aCDOM as a function of SSS for the points within the black contour of a). Data are from CCI Ocean Color v6.0, and CCI SSS v3.2. c), d) : Same as a), b) but using data from CCI SSS v4.4

To check the sensitivity of our results, we redid the same work with the new CCI SSS v4.4 (Figure 6c,d). We can see that the correlations between SSS and aCDOM are a bit lower in the new version. Yet, the relationship obtained is very similar. We can note that the CCI v4.4 seems to be slightly less noisy than the CCI v3.2 (R^2 of 0.65 against 0.63) and reaches slightly lower SSS Figure 6b,d).

Similarly, we obtain a second relationship between SSS and TDOM concentration within the model. By combining the two relationships, we can directly link the TDOM concentration to the a_{CDOM} value.

We then conducted a series of sensitivity tests to assess the impact of this new TDOM parameterization, and more generally the impact of TDOM on the Amazon plume productivity. These tests were conducted before the release of the new CCI v4.4 version. Due to the high computational cost of these simulations, the long time it takes to run them, and the fact that CCI v3.2 and CCI v4.4 give similar results, we decided not to re-run the simulations

Before analyzing the results, we validated the TDOM parameterization by comparing the a_{CDOM} of the model (Figure 7a) to the observations (Figure 7.b). We can see that the model reproduces well the observations. It is too low close to the Amazon mouth (2 m^{-1} for the model, vs 5 m^{-1} for CCI observations), but due to the vertical resolution of the model at the surface, this does not

impact the results (the first level of the model is at 0.5 m, which means that all the light is absorbed at the surface anyway).

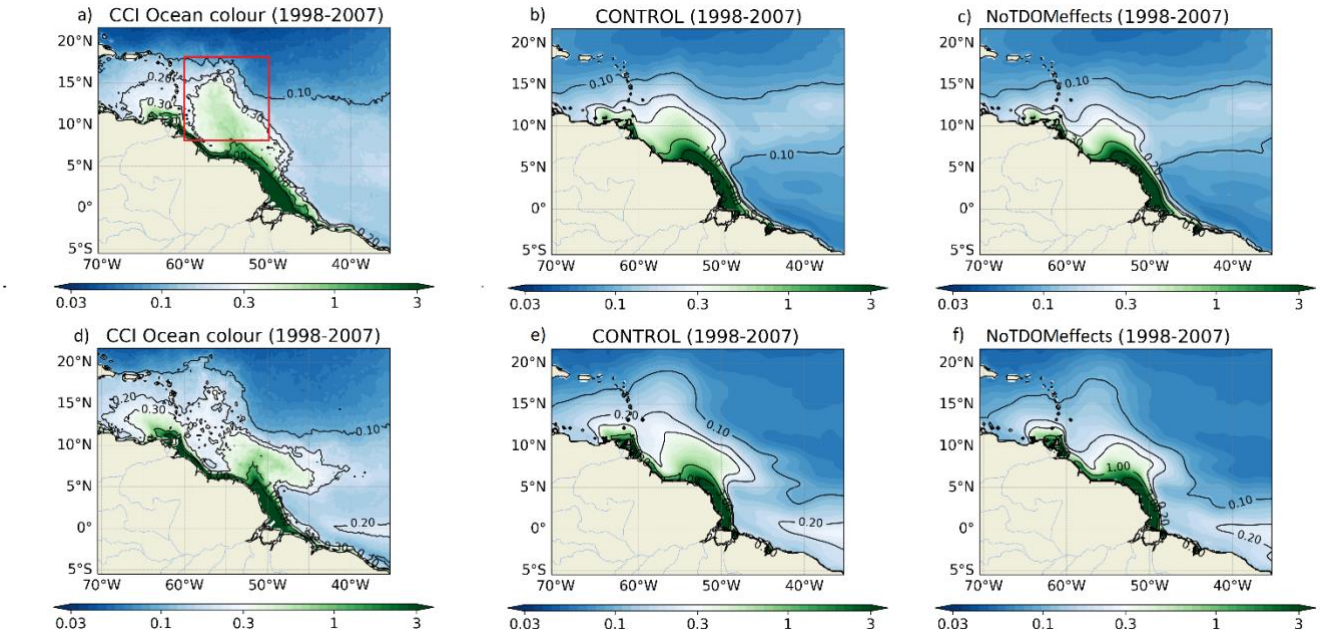

Figure 7 Chlorophyll maps for the spring season (April-May-June) for a) CCI observations, b) simulation including the TDOM effects (specific remineralization and optical effect), c) simulation without the TDOM effects. The red box shows the area of the average for Figure 2.4. d), e), f): same as a), b), c) but for the summer season (July-August-September).

We also validated the good representation of the Amazon plume by observing the SSS of the region (Figure 7c,d). We can see that the model is slightly too fresh, but reproduces well the pattern of SSS, which is satisfactory for our study.

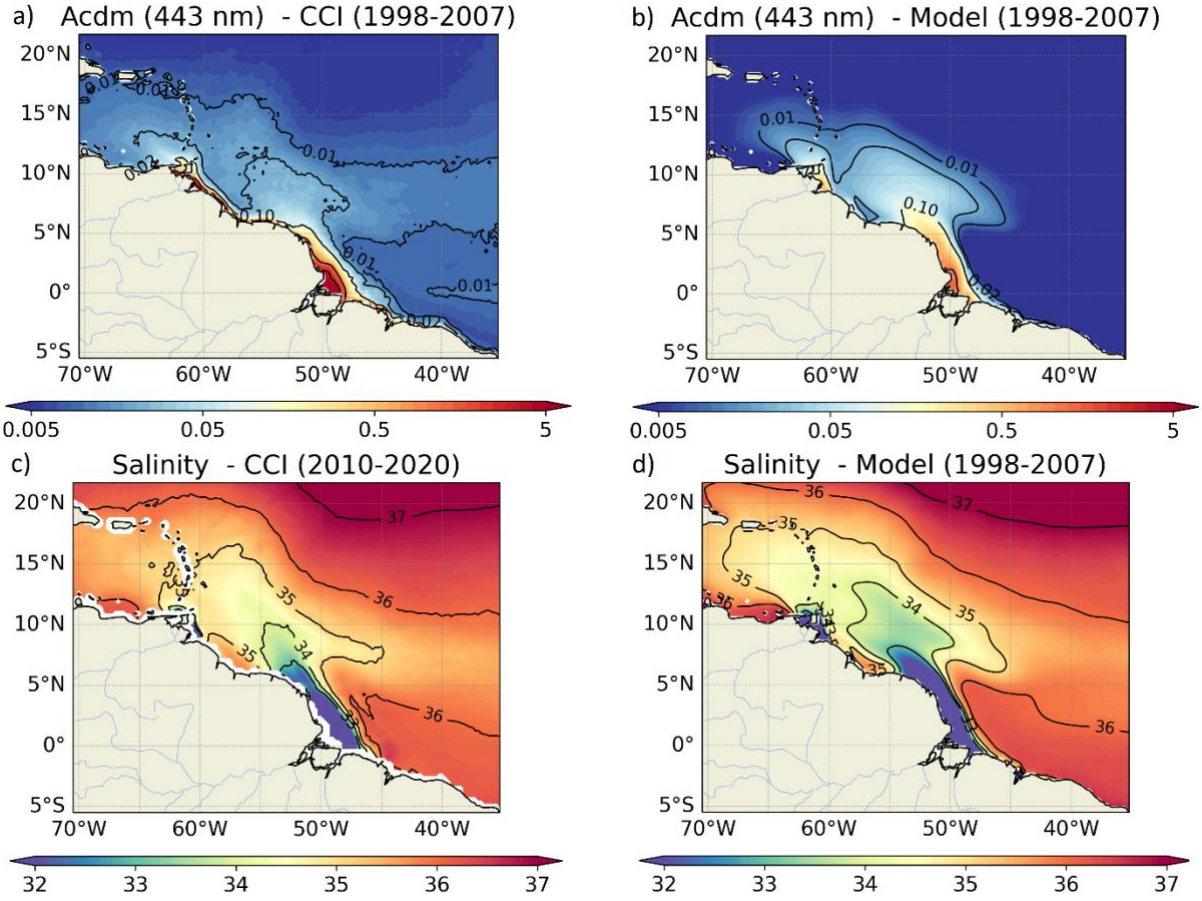

Figure 8 Annual mean of a CDOM for a) CCI observations and b) the model. c), d): same as a), b) but for SSS.

The influence of TDOM parameterization is shown on Figure 8, for the spring season (Figure 8a,b,c) and the summer season (Figure 8d,e,f), the two seasons of strongest phytoplanktonic blooms. We can see that for both seasons, the simulation including TDOM specific remineralization and optical effect (CONTROL, Figure 8b,e) is more able to reproduce the offshore blooms than the simulation without TDOM effects (NoTDOMeffect, Figure 8c,f). This becomes even more evident when examining the time-series of chlorophyll in the offshore part of the plume (Figure 9). The seasonal peaks of chlorophyll are much more accurately reproduced in the CONTROL simulation. However, the interannual variability still needs improvement, as demonstrated by the too low chlorophyll peaks in 2001 and 2007. The too low peaks might be due to the TDOM fluxes that we input into the model. Indeed, these TDOM fluxes are calculated as the product of runoff and TDOM concentration. Runoff are daily interannual values, but TDOM concentrations are only monthly climatological values. Having an interannual variability of TDOM concentration could allow to improve the interannual variability of the chlorophyll peaks.

A final sensitivity test was performed, in which we completely removed the TDOM fluxes (green curve on Figure 9). We can see that the chlorophyll decreases drastically in the offshore part of the plume, which shows the importance of TDOM for the offshore export of nutrients, and the accurate representation of the full extension of the colored and productive plume.

To conclude, this newly developed coupled ocean-biogeochemical configuration is giving very satisfactory results, especially compared to the state-of-the-art models. It will allow to study the influence of SSS on the seasonal phytoplanktonic blooms, and more specifically the impact of the strong salinity stratification induced by the Amazon plume. We can note however that the study

of the impact of the interannual variability of the Amazon River on the chlorophyll would need a further improvement of the model.

A paper on this study is in preparation for Geophysical Research Letters.

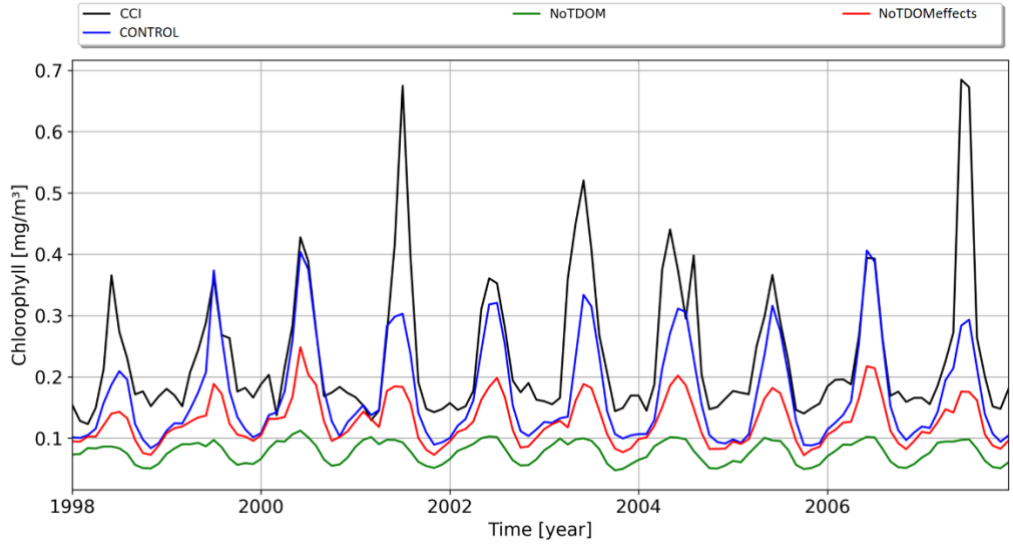

Figure 9 Time series of chlorophyll between 1998 and 2007, for CCI observations (black), CONTROL simulation with all TDOM effects (blue), the simulation without TDOM effects (red), the simulation without TDOM discharge (green). The average is made on the offshore part of the Amazon plume (see red box on Figure 2.3a).

3 ARTIC REGIONAL CASE STUDIES

3.1 Sea Surface Salinity Polar Front variability in Barents Sea from in situ and satellite missions (*N. Kolodziejczyk)*

Contributors : Nicolas Kolodziejczyk, Camille Lique, Jacqueline Boutin, Jean-Luc Vergely, Gilles Reverdin

Climate relevance of this study. Understanding the mechanisms controlling the Polar Front's dynamics and its sensitivity to sea ice variability is crucial for assessing the Barents Sea's response to climate change. The analysis of CCI+SSS observations allows to gain new insights into the role of SSS in shaping the Polar Front's intensity and its connection to sea ice variability. It shows that local sea ice melting contributes to the interannual changes in SSS and Polar Front intensity. Ice coverage and volume during late summer likely influence the strength of the Polar Front.

The Barents Sea is the place of intense exchange between Atlantic and Arctic water masses and an hot spot for water mass transformation due to air-sea fluxes and oceanic mixing processes. It is also a site of Intermediate Arctic Water formation, which feeds the deep branch of the Atlantic Meridional Overturning Circulation (AMOC). On the top of that, under the recent global warming Barents Sea is getting more and more warm and salty due to increase of incoming Atlantic water, but also to weakening of sea ice import from the North.

The Polar Front in the Barents Sea is characterized by a strong Sea Surface Salinity (SSS) and Sea Surface Temperature (SST) gradient separating the cold and fresher Arctic waters from the warmer and saltier Atlantic waters originating from the North Atlantic and Nordic seas. The cyclonic geostrophic circulation associated with the subpolar front is strongly constrained by bathymetry. Previous studies have shown that the position of the SST subpolar front is correlated with bathymetry in the Barents Sea.

The Polar Front is thus known to transitioning the "alpha" to "beta" ocean, i.e. where stratification (water column stability) and density gradients are controlled by temperature and salinity, respectively. In this transition region, salinity becomes the parameter that controls density, and therefore dynamics, all the more so as the intense freshwater flows linked to the seasonal melting of the Sea Ice contribute to the high variability of the SSS in this region.

Advances in L-Band satellite data processing, the synergy of SSS from satellites measurement (Aquarius/SMOS/SMAP in the framework of CCI+SSS v4.4 product) and in situ measurements (at lower resolution) have improved the signal-to-noise ratio of SSS in cold SST regions. The interannual variability of SSS in Barents Sea can be now monitored with a reduced bias and error of the order of 0.5 pss, providing new and more "synoptic" insights into the mechanisms of SSS variability in relation to local freshwater cycle.

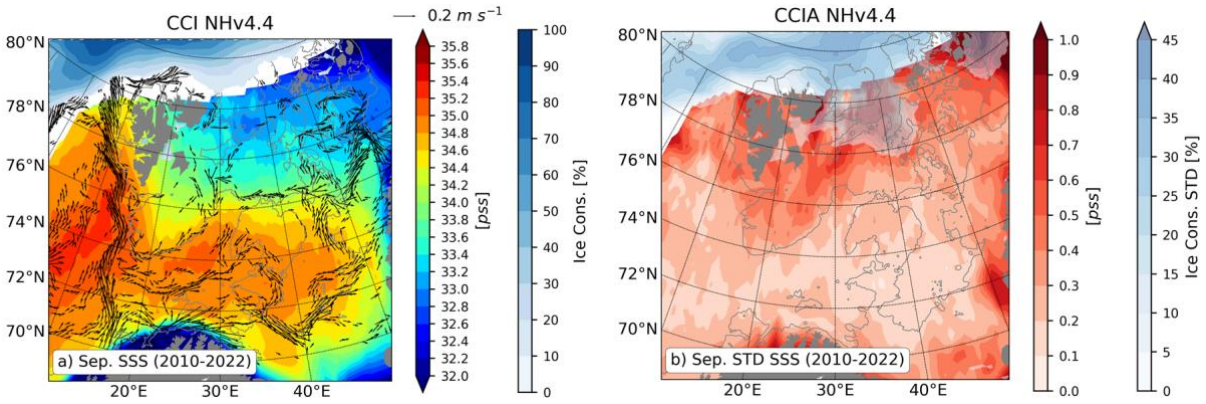

Figure 10. a) Mean September SSS (pss) over 2010-2022 from CCI+SSS along with average September Sea Ice Concentration (%) over the same periods (blue shading). The arrows are the surface GLORYS currents. Only |v|>0.05 m s-1 are shown to enhance the main branches of the surface currents in the Barents Sea. b) SSS September Standard Deviation (STD) from CCI+SSS along with STD September Sea Ice Concentration (%) over the same periods (blue shading). Gray contours indicate the 250 m isopbath.

The results from SSS satellites analysis have enabled us to better characterize the synoptic distribution of SSS (Figure 10a) and its interannual variability (Figure 10b) in Barents Sea during late summer over the period 2010-2022. Fort the first time, both SSS and SST signature of the Polar Front can be compared. This analyses of revealed that the during late summer salinity mainly explained the density signature of Polar Front east of 30°E (Figure 11).

At interannual time scale, the SSS variability in September is intensified north of the Polar Front (Figure 10b). At this location, the SSS interannual anomalies exhibit strong year-to-year changes (Figure 12), associated to consistent scenario of sea ice coverage: the years with negative (positive) September SSS anomalies north of the front, later (sooner) and less (more) northward retreat of the Sea Ice are observed during late summer, e.g. 2017 or 2014 (2018) in Figure 12. We have shown that the interannual anomalies of SSS north of the Polar Front explained the interannual variability of the intensity of the Polar Front.

We have hypothesized that the local melting of the Sea Ice is likely to provide surface freshwater flux explaining the interannual change of SSS and Polar Front intensity in the northern Barents Sea. In other words, the Sea Ice coverage and volume during late summer may be correlated with the intensity of the front. We have shown the relationship between Ice coverage and intensity of Polar Front, and assess the amount of melt water explaining the drop of salinity north of the Polar Front from Sea Ice thickness and SSS products. These results shows that L-Band SSS allows to monitor the low SSS associated with melting and freshwater cycle in the ice-free regions of the Arctic Ocean.

An article presenting these results is currently in preparation for Journal of Geophysical Research and will be submitted by the end of 2023.

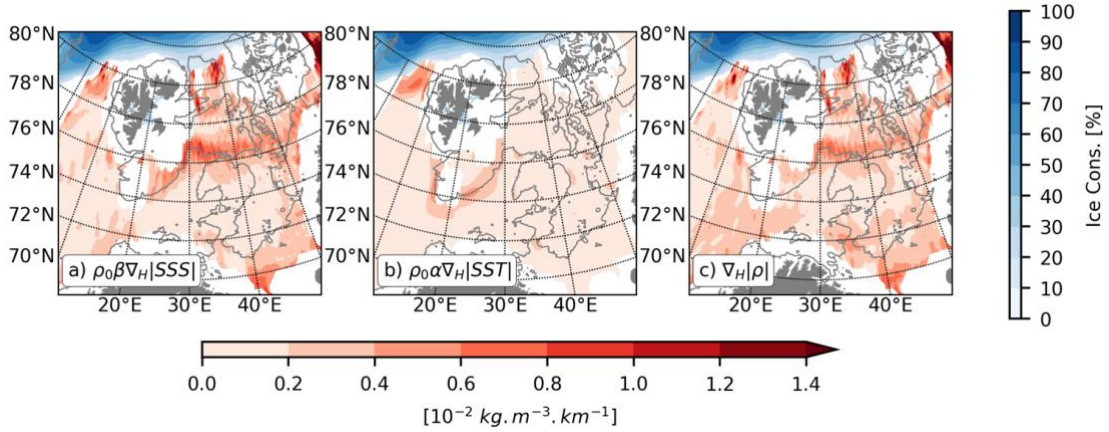

Figure 11 Mean September norm of equivalent density horizontal gradient for a) SSS gradient, b) SST gradient, and c) computed density gradient (kg.m-3.km-1) over the period 2010-2022. Mean September Sea Ice Concentration between 2010-2022 is indicated in blue (in %).

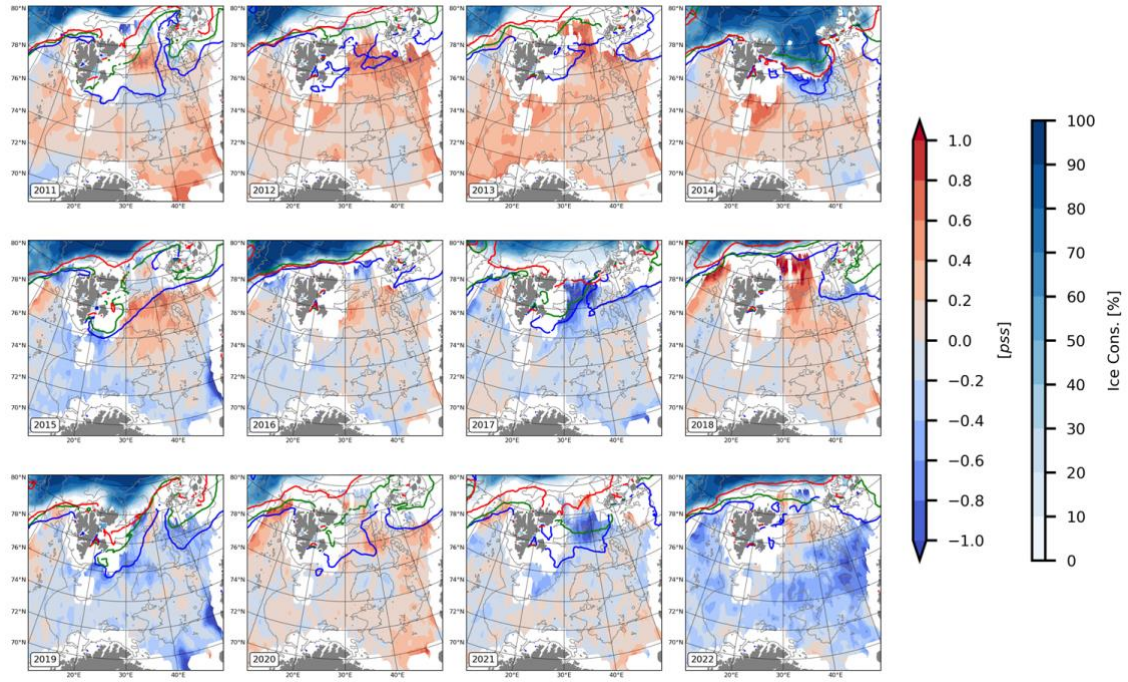

Figure 12 September CCI SSS anomaly (blue/red shading) and AMSR2/E Sea Ice Concentration (blue shading) during the period 2011-2022. SIC edge (15%) is shown in contour for June (blue), July (green) and august (red).

3.2 Impact of freshwater anomalies on Barents Sea dense water formation inferred from model reanalysis (*R. Raj*)

Contributors : Vidar. S. Lien, Roshin. P. Raj, Laurent Bertino

Climate relevance of this study: The eastern subpolar North Atlantic underwent extreme freshening during 2012 to 2016, with a magnitude never seen before in 120 years of measurements. The signature of the freshening has also been found to extend further north in the Norwegian Basin and the Lofoten Basin. We investigate the propagation of freshwater anomalies into the Barents Sea and its impact on the salinity and the freshwater content of the region using TOPAZ reanalysis dataset and CCI+SSS observations.

The Barents Sea is the largest shelf sea that is adjacent to the Arctic Ocean, and it accounts for a substantial part of the dense water that is formed within the Arctic (Martin & Cavalieri 1989). In

the Barents Sea, the poleward flowing Atlantic Water undergoes considerable modifications and eventually enters the Arctic through the St. Anna Trough (e.g., Schauer et al., 2002), thereby contributing to the renewal of the intermediate and deep water in the Arctic Ocean (Rudels et al., 2000). Several processes contribute to the modifications of the Atlantic Water within the Barents Sea (Ozhigin & Ivshin 1999; Rudels et al. 2004). In recent years, the salinity of the North Atlantic has decreased to the lowest level in the instrumental record (Holliday et al., 2020). Subsequently, the salinity of the Atlantic water flowing through the Norwegian Sea has also decreased, while the temperature, on the other hand, has increased or remained relatively high (Mork et al., 2019; Skagseth et al., 2020). The result is a decrease in the density of the Atlantic water upstream of the main areas of dense water formation feeding into the overflow water that exits the Nordic Seas to the North Atlantic. Here, we investigate the impact of the recent changes in the Atlantic Water hydrography on the freshwater content (FWC) of the Barents Sea. Analysis also focuses on the role of the atmospheric forcing on the FWC of the region, and the impact of the freshening on the dense waters exiting the Barents Sea to the Arctic via the St. Anna Trough and to the Norwegian Sea through the Barents Sea Opening.

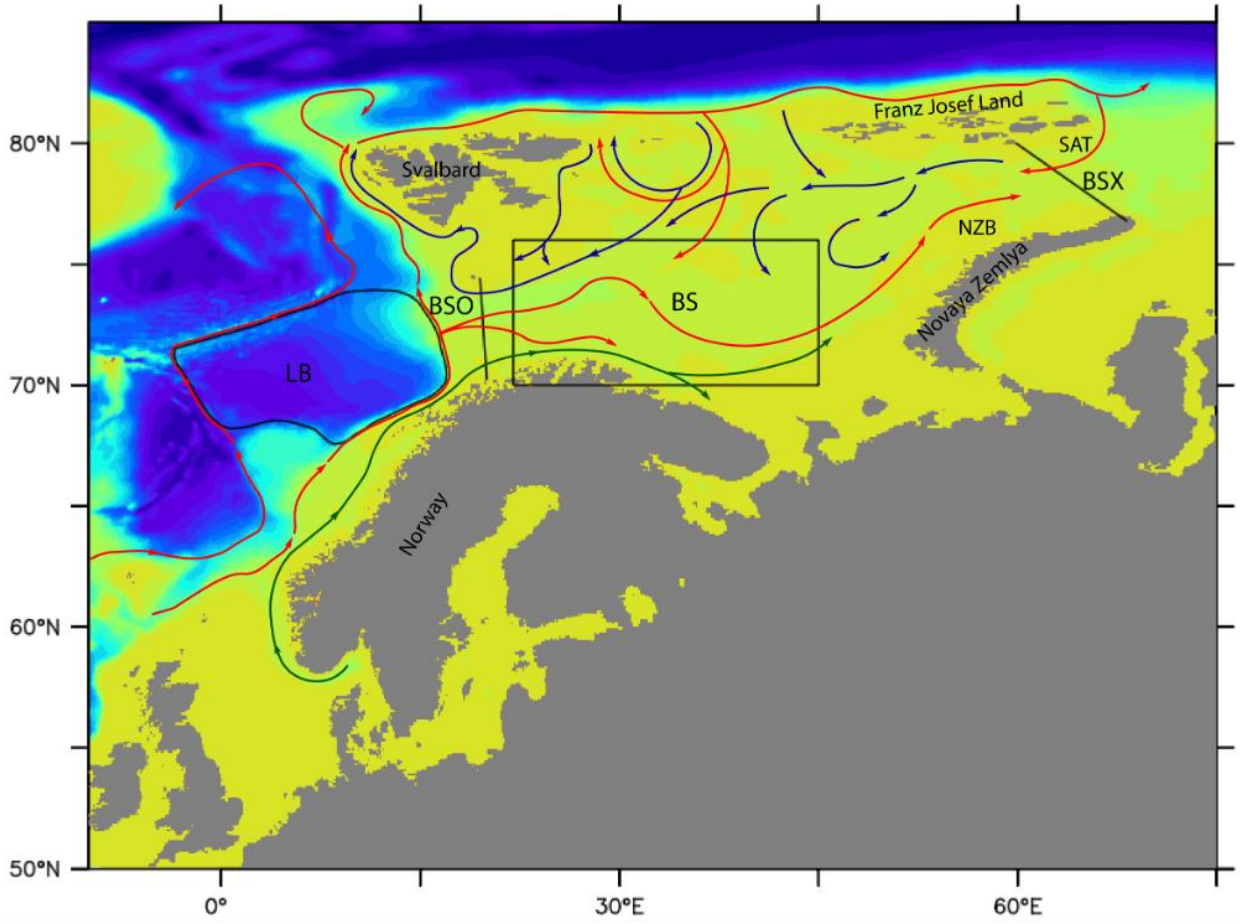

Figure 13 Map of the investigation area. Arrows show the main circulation patterns. Red arrows: Atlantic water. Blue arrows: Arctic water. Green arrows: Coastal water. LB: Lofoten Basin. BS: Barents Sea. BSO: Barents Sea Opening. BSX: Barents Sea Exit.

Data used: **(1)** TOPAZ4, a coupled ocean and sea ice data assimilation system for the Arctic based on the HYbrid Coordinate Ocean Model (HYCOM), with 50 hybrid z-isopycnal layers at a horizontal resolution of 12 to 16 km, uses the ensemble Kalman filter method (EnKF; Evensen 2003) to assimilate consistently multiple types of observations in the ocean and sea ice (Xie et al., 2016). TOPAZ4, forced by ERA5 reanalysis, assimilates observations such as including along-track altimetry data, sea surface temperatures, sea ice concentrations and sea ice drift from

satellites along with in situ temperature and salinity profiles. **(2)** Monthly ERA-5 mean sea level pressure data for the time-period (1993-2020) is used in this study to investigate the role of large-scale atmospheric forcing. **(3)** ARMOR3D gridded salinity observation data used contain multi-year, reprocessed 3D temperature and salinity at ¼ degree regular grid and 50 depth levels from surface to 5500 m depth (or the ocean bottom) at a temporal resolution of one month. **(4)** ESA CCI SSS data (Version 4.4).

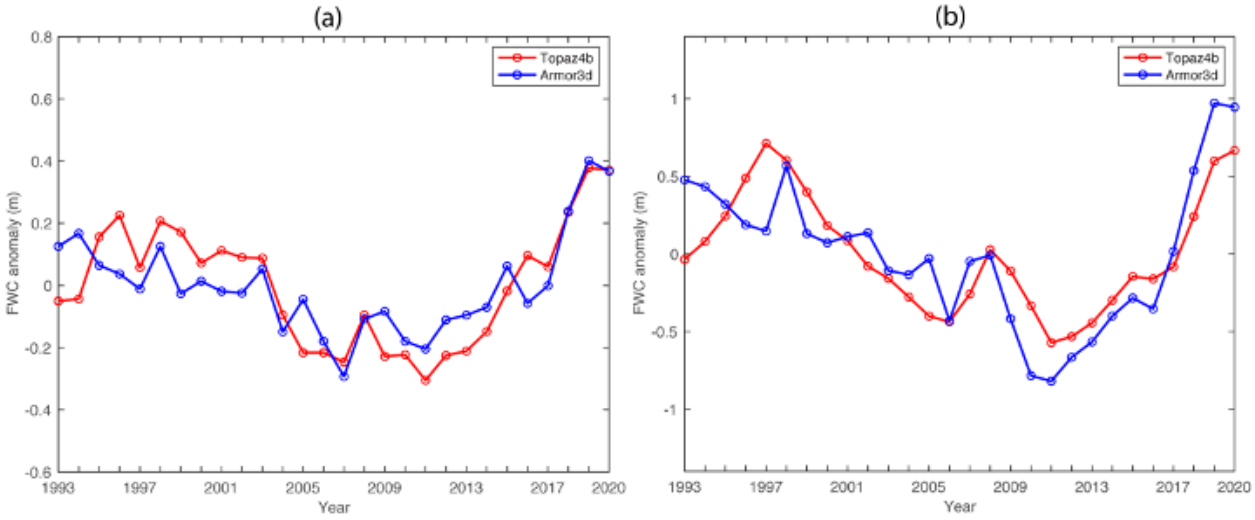

Figure 14 Annual mean freshwater content anomaly in the a) Barents Sea (full depth) and b) in the Lofoten Basin (upper 1000 m).

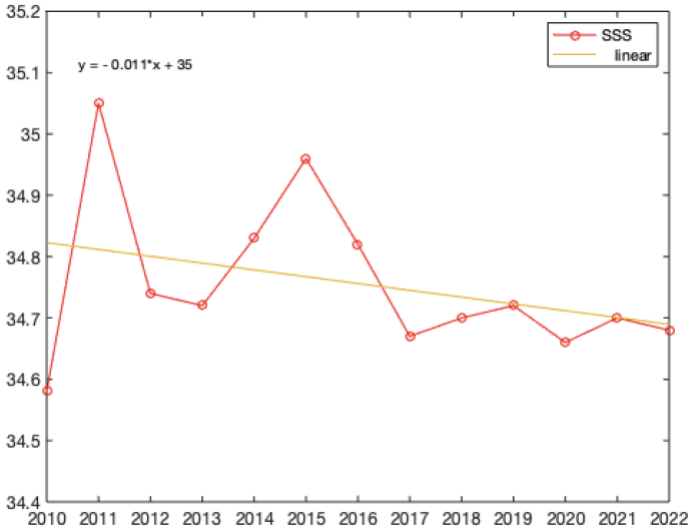

Figure 15 Annual variability of satellite derived SSS in the Barents Sea during the time-period 2010-2022.

Figure 14 shows modeled and observed depth-integrated (surface to bottom) freshwater content anomaly (w.r.t mean 1993-2020 FWC) in the Barents Sea. The area used for the estimation of the FWC anomaly roughly corresponds to the southwestern Barents Sea (i.e., the Atlantic water dominated part of the Barents Sea; Figure 13). According to both the model reanalysis and gridded in-situ data product, the FWC during the period 1993-2020 was the highest after 2017. This result is in agreement with the reported freshening of the northern North Atlantic in the years 2012-2016 (Holliday et al., 2020), accounting for a propagation speed of 2-3 cm/s within the Nordic Seas yielding a time lag of approximately 2-3 years between the inflow region to the Nordic Seas and the Barents Sea Opening (Furevik, 2001; Sundby & Drinkwater, 2007; Årthun & Eldevik, 2016). The FWC estimates (upper 1000m depth) of the Lofoten Basin, located directly upstream of the Barents Sea (Figure 14b) show negative and positive trends during the two decades D1 and D2, respectively. Furthermore, a statistically significant correlation ($r = 0.86$; $p <$

0.01) is found between the annual mean FWC time series of the Lofoten Basin and the Barents Sea. Such coherence is to be expected since the Norwegian Atlantic Slope Current is transporting Atlantic Water into both the Lofoten Basin and the Barents Sea.

The variability in the surface salinity of the BS region (Figure 13) derived from satellite derived SSS (Figure 15) also showed the signature of increased freshwater influence since 2010. Further analysis (a regression analysis of sea level pressure over the Nordic Seas and TOPAZ model derived freshwater transport through the Barents Sea Opening) suggests that the atmospheric conditions during the most recent decade, D2 (2011-2020), tended to favor stronger inflow to the Norwegian and Barents Seas compared to the decade D1 (2001-2010). A North Atlantic Oscillation-like pattern was found during period D2, where the atmospheric pressure gradients were much stronger and aligned parallel to the Norwegian coast, thereby facilitating a strong northward flow along the coast, compared to the pressure gradients during D1. The model results further indicate coherent changes in FWC throughout the water column in the Barents Sea (not shown), in agreement with the findings by Skagseth et al. (2020) that Barents Sea temperature anomalies show vertical coherence.

3.3 Role of atmospheric forcing on the variability of the surface salinity of the Barents Sea (*R. Raj*)

Contributors : Roshin. P. Raj, Lluisa. Pong. Moner, S. Chatterjee, Laurent Bertino, Vidar. S. Lien

Climate relevance of this study: Ocean fronts in the Nordic Seas and the Barents Sea, like its counterparts in the world ocean, are important biologically productive regions also known for its large feeding schools of pelagic fish (e.g. Holst et al., 2004; Blindheim and Rey, 2004; Melle et al., 2004). On its influence on higher trophic levels, it is important to note that Jan Mayen Island located near the Arctic Front in the Nordic Seas is an important breeding region inhabited by large colonies of seabirds (Norway Ministry of Environment, 2008–2009). We investigate the variability of the ocean fronts in the region using a suite of satellite data (sea surface salinity, sea surface temperature, sea surface height), and TOPAZ reanalysis, applying advanced methodologies such as Singularity exponent analysis.

Data used: (1) ESA CCI SSS data (NH, Version 4.4); (2) Monthly ERA-5 mean sea level pressure data for the time-period (1993-2020) is used in this study to investigate the role of large-scale atmospheric forcing; (3) Cryo-TEMPO and CMEMS altimeter data; (4) ESA CCI SST data.

Methodology:

(1) Singularity analysis: Singularity analysis aims to obtain a dimensionless measure known as the singularity exponent at each point, which represents the degree of irregularity at that location. Singularity exponents are dimensionless and can be derived from any scalar quantity, e.g. SST (Turiel et al., 2009) and wind components (Portabella et al., 2012; Lin et al., 2014). A singularity exponent is a continuous extension of classical concepts such as continuity or differentiability. The main difference between the maximum gradient method and singularity exponents is that singularity exponents are normalized so that the absolute value of the gradient is irrelevant. What is important is the degree of correlation between nearby gradients: singularity exponents are the dimensionless measures of that correlation. Hence the results from the singularity analysis of different scalar variables (for, e.g., SST and wind speed) can be directly compared. Furthermore, singularity analysis does not require knowledge of the velocity field, because it is a Eulerian method exploiting the scaling properties of the spatial correlations of the gradients of a

given scalar field. Thus, singularity analysis has an advantage over the use of Lyapunov exponents (Garcia-Olivares et al., 2007), another widely used methodology which requires the velocity field to be known.

(2) EOF analysis: The monthly detrended and de-seasoned ERA Interim MSLP data are used to calculate the three-leading empirical orthogonal functions (EOFs) of atmospheric variability in the North Atlantic (80◦ W to 50◦ E and 30 to 80◦ N), which are based on singular value decomposition, according to the method described by Hannachi et al. (2007). The data are weighted by the cosine of their latitude at every grid point of the study region to account for decreasing grid sizes towards the pole. The three leading modes of atmospheric variability in the North Atlantic are the North Atlantic Oscillation (NAO), the East Atlantic Pattern (EAP) and the Scandinavian Pattern (SCAN). (3) Composite analysis: For composite analysis, the positive/negative phase of the NAO (NAO+/NAO−) are categorised as those months with NAO index values above/below one standard deviation calculated over the entire period from 1991 to 2021. Similarly, the positive/negative phase of EAP and SCAN are estimated from their respective time series.

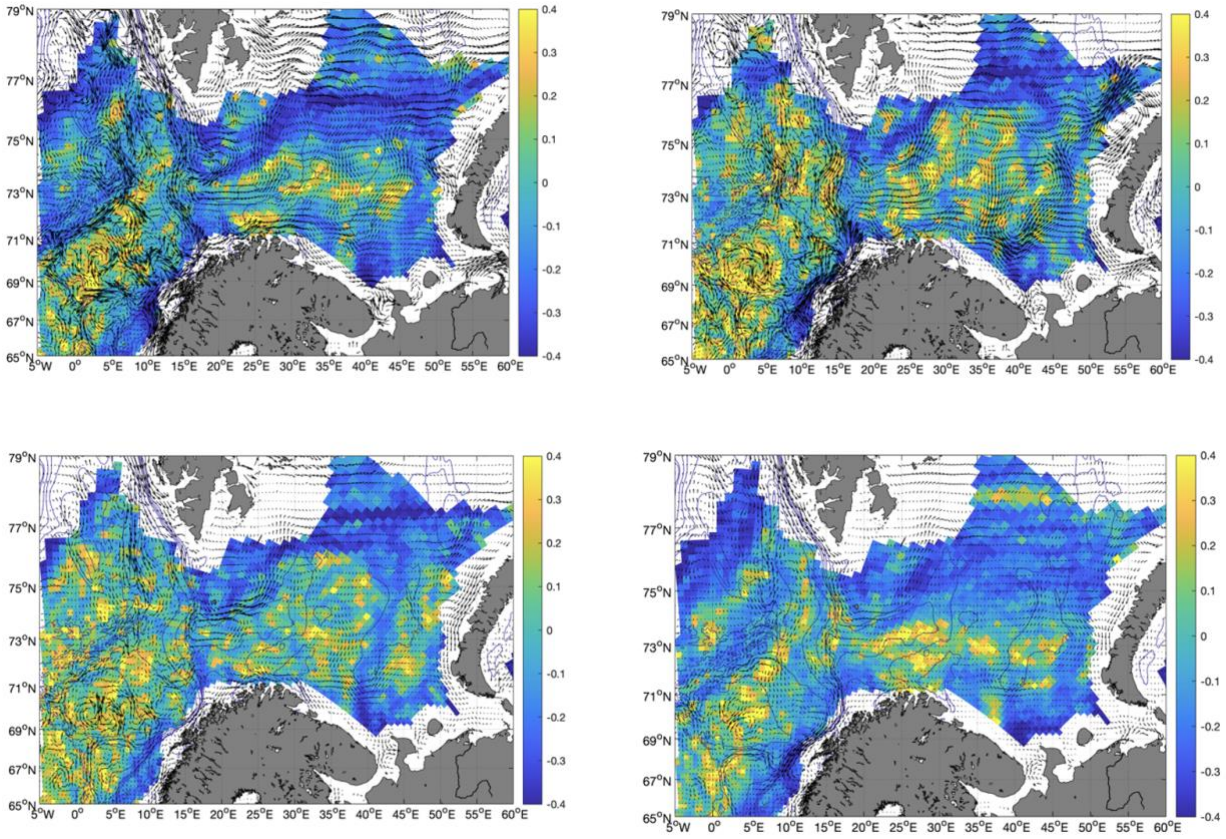

Figure 16 Singularity exponents (color) estimated from mean SSS (2010-2022) during: Autumn (top left panel); winter (top right panel); spring (bottom left panel); summer (bottom right panel). Mean geostrophic velocity anomalies estimated from sea level anomalies for the respective seasons are overlayed.

Figure 16 shows the singularity exponents, which provides information about the local regularity (if positive) or irregularity (if negative). In simple terms regions with high negative values are regions where there is a sharp gradient. Figure 16 reproduces all main circulation features of the Norwegian and the Barents Sea. The seasonal variability of the front in the Barents Sea (75°N to 77°N) resulting from the interaction of cold and less saline Arctic Waters transported from the east and the warmer/more saline Atlantic Water is of particular interest. All-in-all, the location

of the fronts and its seasonal variability derived from the SSS singularity exponents matches very well with the altimeter derived velocities.

Next Steps: (a) Focus separately on the SSS variability in the Barents Sea and the Norwegian Sea. **(b)** Composite analysis to delineate the effect of the dominant atmospheric modes on the SSS variability in the Barents Sea and the Norwegian Sea separately.

4 IMPROVEMENT AND ASSESSMENT OF THE REPRESENTATION OF SSS IN OCEAN REANALYSIS

4.1 Data assimilation of SSS and impact on an ocean reanalysis (M. Martin)

Climate relevance of this study. SSS is an important indicator of climate variability and change. Assimilating SSS data into reanalysis is expected to improves the model's ability to simulate climate anomalies and long-term trends, such as those associated with El Niño-Southern Oscillation (ENSO) and global climate change. It can potentially results is a more accurate representations of the surface currents, water mass transformation, and stratification of the upper ocean, and thus in a deeper understanding of the Earth's climate system.

The aim of this case study is to build in the work described by Martin et al. (2019) – hereafter referred to as M19 - and Martin et al. (2020) who demonstrated the impact of assimilating satellite SSS data on operational ocean forecasting systems. We focus here on the system at the Met Office and aim to update the data assimilation (DA) and forecasting system so that it makes use of the latest developments in model and DA since those earlier papers, uses updated versions of the satellite SSS datasets, and improves the assimilation of satellite SSS data. Once these activities have been carried out, we will run a 5-year reanalysis to understand the impact of new SSS datasets.

Model and data assimilation overview

The Forecasting Ocean Assimilation Model (FOAM) system is used at the Met Office for operational ocean and sea-ice forecasting (Barbosa Aguiar et al., 2023), as part of a coupled NWP system, and for ocean reanalysis. The model component of the system has recently been upgraded to NEMOv4.0.4 which includes a new sea-ice model (SI^3) and the model state variables have been changed to those of the TEOS-10 equation of state: the temperature variable is now conservative temperature and the salinity variable is absolute salinity. Changes have been made to the observation operator in NEMO to convert between practical salinity and absolute salinity.

We use a 3DVar-FGAT (first guess at appropriate time) DA algorithm using the NEMOVAR software. Various DA improvements have also been made to the configuration of NEMOVAR compared to the system used in M19 including a change to the horizontal length-scales used to spread temperature information. Only a single, Rossby-radius dependent, length-scale is used for temperature instead of the two length-scales used previously which has been shown to improve the overall accuracy of the short-range forecasts. Two length-scales were retained for salinity however, because removing the large-scale corrections for salinity resulted in larger biases near the surface when only in-situ profiles of salinity are assimilated.

Satellite SSS observation pre-processing and bias correction

The satellite SSS datasets used here are from SMOS and SMAP and we aim to use L2 data since the FOAM system normally runs on a daily cycle and includes an observation bias correction scheme to estimate and remove biases in different satellite products, as described by M19. Given the biases in the ascending and descending passes are likely to be different, we process the data into separate datasets for SMOS ascending/descending and SMAP ascending/descending passes on each day so that the biases can be estimated separately for these four groups. The observation

biases are estimated online as part of the DA in a variational bias correction algorithm using the near-surface Argo salinity data (< 5 m depth) as an anchor dataset (assumed to be unbiased).

SMOS data are obtained from CATDS and are described by Boutin et al. (2018) and on the CATDS website[1]. It was reprocessed in Feb 2022 and contains the full SMOS timeseries. The L2Q product which we use is an intermediate product, that provides, in daily files, SSS corrected for land-sea contamination and latitudinal bias. Ascending and descending orbits are processed separately. The data have been converted into the format needed for assimilation, during which there is some selection of the data as summarised in Table 2.

The SMAP data are obtained from REMSS[2] and are described in Meissner et al. (2022). We use version 5.0 of the data and select the data filtered with a 40 km length-scale. To select data, we follow the instructions in the user manual[3] (described in Table 4 and Section 7) where they describe how the L3 product is generated. We do not include the temporal averaging aspects of their L3 product generation but use the same selection of QC flags as their L3 product generation, excluding the rain filtering of the data. We split the data into separate daily files for ascending/descending passes.

Selection criterion	SMOS	SMAP
Source	CATDS	REMSS
SSS variable	Sea_Surface_Salinity	sss_smap_40km
SSS error variable	Sea_Surface_Salinity_Error	sss_smap_40km_unc
Latitude	< 40° N/S	< 40° N/S
Swath selection	< 400 km of nadir	None
QC flag selection	Sea_Surface_Salinity_QC=0	As the L3 processing described in user manual
Error rejection	< 1 pss	< 1 pss

Table 2 Selection of satellite SSS data from SMOS and SMAP. For SMAP the fore and aft looks are averaged together.

Experimental set-up

Several short experiments have been carried out to test the impact of different aspects of the SSS DA on the resulting analyses. These were run with the eORCA025 configuration (approximately 1/4° horizontal resolution) with 75 vertical levels where the top level represents the top 1 m of the ocean. The surface forcing was from the Met Office NWP system, the river forcing was from a monthly climatological dataset and the initial conditions on 9th Jan 2020 came from a previous reanalysis which assimilated standard observation datasets (SST, SLA, T/S profiles and satellite sea ice concentration). The control experiment assimilated only these standard datasets, while the other experiments assimilated the satellite SSS datasets described above. Table 3 summarises the main experiments.

[1] http://dx.doi.org/10.12770/12dba510-cd71-4d4f-9fc1-9cc027d128b0
[2] https://www.remss.com/missions/smap/salinity
[3] https://data.remss.com/smap/SSS/V05.0/documents/SMAP_NASA_RSS_Salinity_Release_V5.0.pdf

Experiment name	Description	SSS data	
		SMOS	SMAP
control	Standard FOAM system	N	N
sss_assim	As *control* but with assimilation of SMOS/SMAP as in M19	Y	Y
sss_assim_smosonly	As *control* but including assimilation of SMOS	Y	N
sss_assim_smaponly	As *control* but including assimilation of SMAP	N	Y
sss_assim_nosssbias	As *sss_assim* - without SSS bias correction	Y	Y
sss_assim_distcoast	As *sss_assim* - obs errors are 2x expected values within 100 km of the coast	Y	Y
sss_assim_reperr2	As *sss_assim* - with 2x representation error std. deviation	Y	Y
sss_assim_1scaleS	As *sss_assim* - salinity background error correlations horizontal length-scale based on the Rossby radius	Y	Y
sss_assim_reperr2_1scaleS	As *sss_assim* – 2x representation errors and a single horizontal scale for salinity	Y	Y
sss_assim_reperr2_1scaleS_20deg	As *sss_assim_reperr2_1scaleS* - only assimilating the SSS data equatorward of 20° N/S	Y	Y

Table 3 Description of assimilation experiments carried out.

Estimates of observation biases

Figure 17 shows the estimates of the bias in each of the SMOS and SMAP ascending and descending observation types. These are from the *sss_assim* experiment and averaged over Feb 2019. The SMOS biases are large and negative in the N. Pacific for the ascending data, particularly in a latitude band between 20-40°N. There is a corresponding band of large positive biases in the descending data in the western N. Pacific in that latitude range, but the picture is more complicated in the eastern N. Pacific. The descending SMOS biases are large and positive in the eastern Pacific between 30°S and 30°N. In the N. Atlantic the descending SMOS biases are positive in a latitude band between 20-30°N. The biases in the Indian Ocean have quite a complex structure, particularly in the ascending SMOS data. The SMAP biases are quite similar in ascending and descending passes. As for SMOS, they have large values in the N. Pacific and Atlantic in a latitude band between 20-40°N. There are similar large biases in the 20-40°S latitude band with a particularly large area of bias in the southern Indian Ocean.

To make sure that the SSS bias correction methodology is really improving the quality of the analysis, we removed it while keeping everything else the same. The resulting percentage change in the RMS difference (RMSD) compared to in situ profiles of salinity is shown in Figure 18a. There is a clear degradation when removing the SSS bias correction confirming that we should maintain this part of the assimilation methodology.

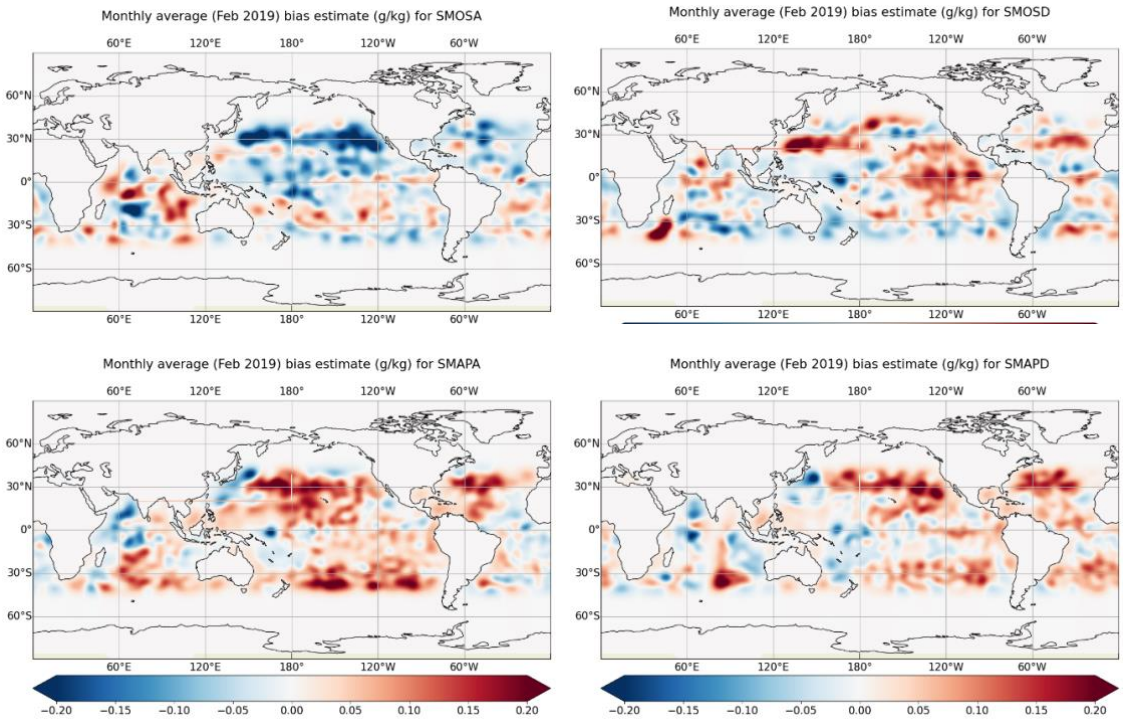

Figure 17 Monthly average estimates of the bias in the satellite SSS data (g/kg) for Feb 2019 from the sss_assim experiment. The top row is for SMOS and the bottom row is for SMAP; the left plots are for the ascending passes and the right plots are for the descending passes.

Representation error

The SSS observations represent processes which are not represented in the model so we include in the assimilation an estimate of representation error to avoid overfitting high resolution features in the observations. In M19 we used a value of 0.5 g/kg for the representation error in SSS data. We estimated the representation error here by calculating the sub-grid scale variability in the SSS observations, following the approach of Oke and Sakov (2008). On each three-day interval, the standard deviation of the observations falling within a model grid box was calculated (not shown). Our previous estimate seems reasonable since these results show the representation errors to vary between about 0.45 and 0.6 g/kg. Nevertheless, we ran an experiment where the representation error standard deviation used in the DA was set to 1.0 g/kg. Figure 18b shows the impact this change has on the RMSD of the model compared to in-situ profile salinity data for Jan 2019. There is a small improvement in the RMSD from this increase in the representation errors so this change should be maintained. Perhaps this result is because the representation errors due to vertical processes are a significant part of the overall representation errors, and these are not captured by the method used to estimate them here.

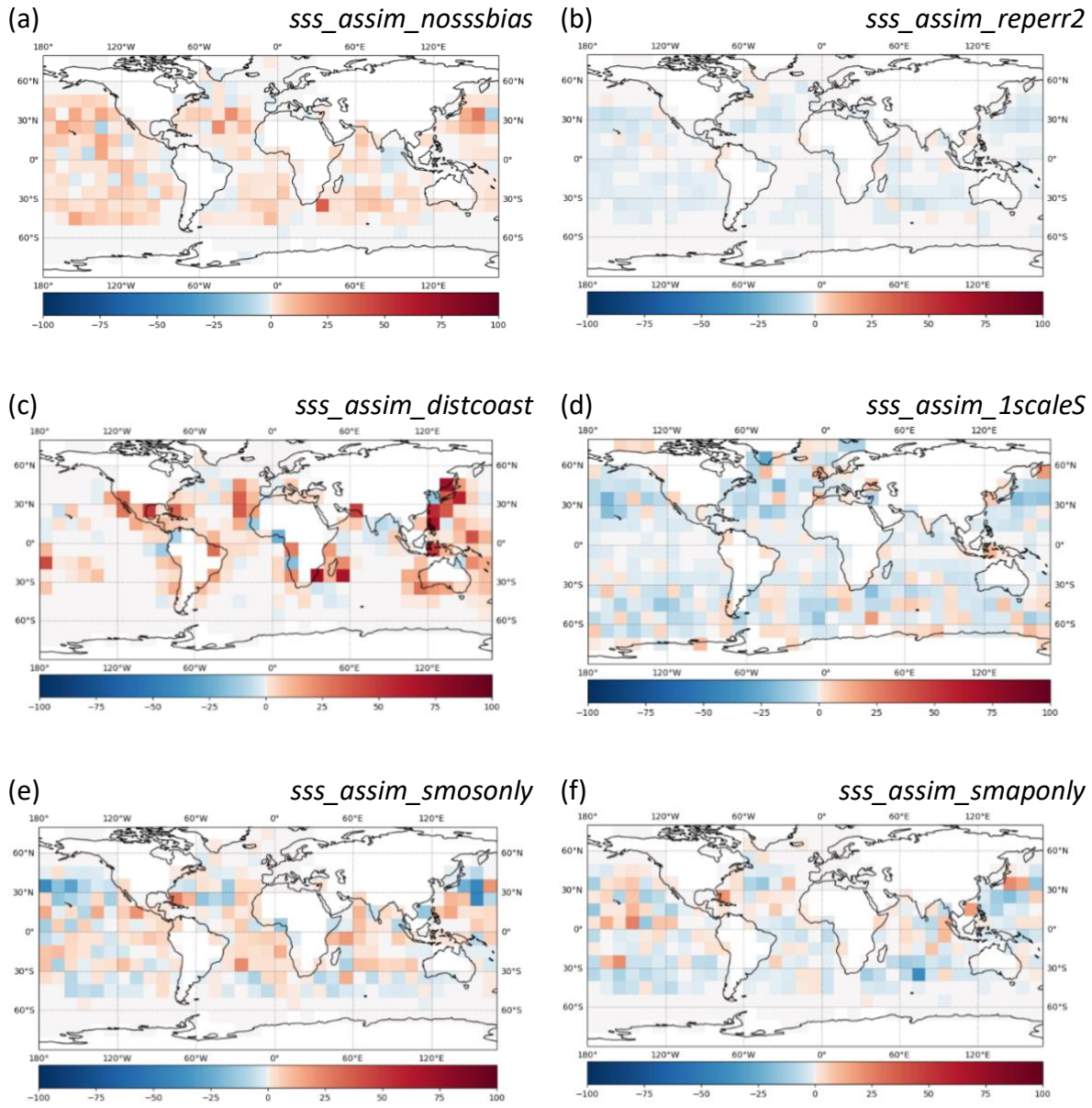

Figure 18 Percentage change in RMSD between the model and the in-situ profile salinity data for various experiments compared to experiment sss_assim over Jan 2019. Positive values mean an increase in the RMSD for each experiment compared to experiment sss_assim.

Impact of SSS data near the coast

In M19 the SSS data were given very little weight near coasts. Observation error standard deviations were artificially increased in the DA so that they reached 10 times the pre-specified values within 800 km of the coast. To test whether we should change this so that the SSS data can affect the model closer to the coast, we changed the settings so that the pre-specified values were doubled within only 100 km of the coast instead. Figure 18c shows the impact this had on comparisons of the model short-range forecast with in-situ profiles of salinity. There are quite large degradations in the results around most of the coasts. There are exceptions, including in the Bay of Bengal as well as around some parts of west Africa where there are some improvements from assimilating the satellite SSS data closer to the coast, but overall this change degrades the results so we maintain the previous settings in this aspect.

Impact of changing the background error correlation length-scales

The background error correlations determine how observation information is spread spatially by the DA. As mentioned earlier, the temperature background error correlation length-scales are based on the first baroclinic Rossby radius with some maximum values in the tropics and minimum values at high latitudes. For salinity, we specify the background error correlation length-scales based on two components, one which is also based on the Rossby radius, and one which is set to 400 km. The weight given to the two components is spatially and seasonally varying. The reason for having a longer length-scale component for spreading salinity information is that the observations (without the satellite SSS data) are sparse compared to the scales of the errors in salinity. When assimilating the satellite SSS data there is an opportunity to revisit this choice. Figure 18d shows that a reduction in the horizontal length-scale for salinity significantly improves the RMSD compared to in situ salinity profiles almost everywhere when assimilating the satellite SSS data.

Impact of SMOS and SMAP separately

The impact of SMAP data on the RMSD of the short-range forecast is shown in Figure 18e. Removing the SMAP data results in an increase in RMSD indicating that the SMAP data helps to reduce the errors in the forecast almost everywhere, the exceptions being around 30° N in the Atlantic and Pacific. Removing the SMOS data (Figure 18f) results in a mixed picture – there are some widespread small improvements to the results without SMOS assimilation, but some regions are degraded, for instance in the central and eastern tropical and N. Pacific and parts of the Indian Ocean and N. Atlantic. Based on this it seems that assimilating SMAP data gives more benefit than SMOS data.

Overall impact of assimilating SMOS and SMAP with updated assimilation settings

Based on the above results we ran a new set of experiments for about 3 months duration which combined the best settings found so far. The main changes compared to the M19 settings were that we doubled the representation errors and used only a single, short horizontal length-scale for salinity. We retained the previous settings near the coast and kept the bias correction as it was. The experiment sss_assim which has the same DA settings as M19 shows a significant degradation in the latitude range 20-40° in both hemispheres compared to the control, particularly in the northern hemisphere, as seen in Figure 19b. These degradations are also seen in the experiment with the improved settings (sss_assim_reperr2_1scaleS) as shown in Figure 19c, though elsewhere there are some improvements from the updated DA settings. We therefore ran an additional experiment where we limited the assimilation of satellite SSS data to within 20° of the equator. This shows more regions where the SSS data is improving the accuracy of the forecast compared to the control experiment as shown in Figure 19d. Figure 20 shows the salinity RMSD of the different experiments as a function of depth. Over the global ocean the experiment sss_assim_reperr2_1scaleS_20deg has a similar level of RMSD to the control while the other experiments show degradations in the upper ocean. For the N. Atlantic region the sss_assim_reperr2_1scaleS_20deg shows an overall improvement down to about 600 m depth compared to the control. The deeper impact is likely due to the change in the horizontal length-scales for salinity rather than the SSS data per se.

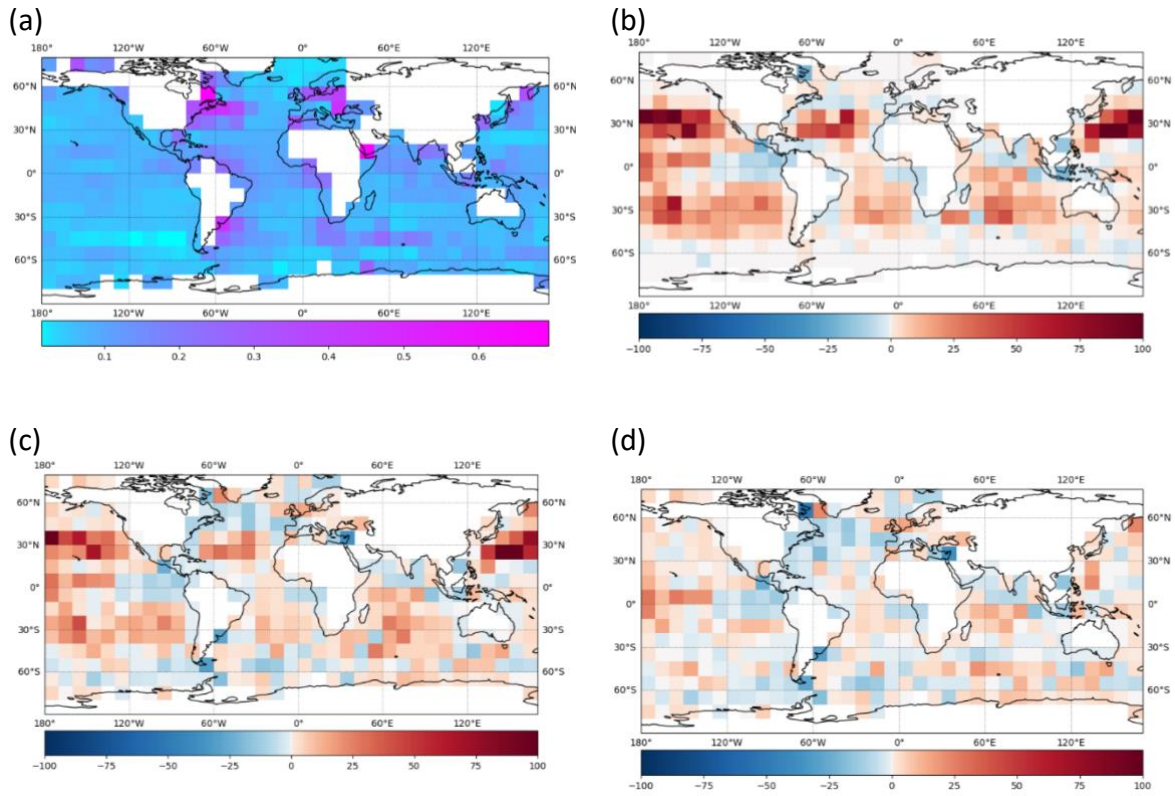

Figure 19 (a) RMS difference of the control experiment compared to in situ profile salinity data (g/kg) over the period 9th Jan to 31st March 2019. The other panels show the percentage change in RMSD compared to the control in experiments (b) sss_assim, (c) sss_assim_reperr2_1scaleS, (d) sss_assim_reperr2_1scaleS_20deg. Positive change means the experiment has a larger RMSD compared to the control.

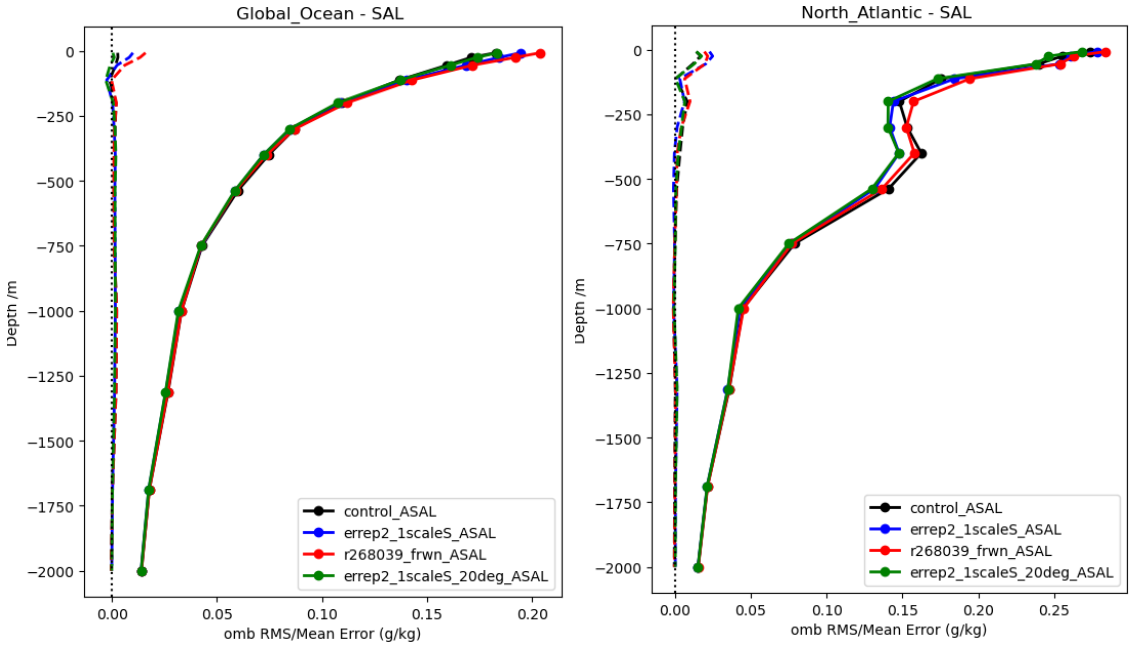

Figure 20 RMS (solid lines) and mean (dashed lines) difference of the model compared to the in situ profile salinity data (g/kg) as a function of depth down to 2000 m in the global region (left plot) and the N. Atlantic (right plot). The black line is the control, red is sss_assim, blue is sss_assim_reperr2_1scaleS, green is sss_assim_reperr2_1scaleS_20deg.

Future work

We have ended up with a configuration for assimilation of SSS data which gives some improvements to the accuracy of the model's SSS field compared to the previous set-up. Some

further improvements could be made, particularly regarding the observation bias correction for the SMOS and SMAP satellite data. The SMOS data has issues with large biases of opposite signs for ascending and descending passes. Finding ways to mitigate these issues in the assimilation of the SMOS data should be the focus of the next part of the work. We also plan to test the impact of increasing the assimilation time-window and cycle length to 5-days compared to the current one day, to see whether the larger number of observations within the assimilation window will lead to a reduction in the random component of the errors as well as a more comprehensive estimate of the observation biases. Once these tests have been carried out, we will begin running longer reanalysis experiments. These will use ERA5 surface forcing and ESA CCI observational datasets for SST, sea ice concentration and altimeter sea level anomalies. We will use the latest versions of the SMOS and SMAP data in discussion with the ESA CCI+SSS project partners.

4.2 Characterization of SSS variability and errors in ocean reanalysis (E. Rémy)

Contributors: Valentin Ruault, Elisabeth Rémy, Gilles Garric, Jean-Michel Lellouche and the MOi team

Climate relevance of this study. Accurate representation of SSS variability and trends in ocean models is essential for producing reliable climate simulations and prediction. This case study contributes to this effort by investigating the trends and main modes of variability of the SSS through the analysis of the seasonal and interannual global patterns of variability.

To assess the variability and trend of the SSS at global scale represented in the Glorys12 reanalysis, we compare it with ESA SSS CCI estimates. We focus our analysis on climate relevant scales: the interannual to seasonal variability over the common period to the two products, 2011-2019. GLORYS12v1 reanalysis (https://doi.org/10.48670/moi-00021) is covering the altimetry era with a horizontal resolution of 1/12° and 50 vertical levels. The 1st level being 1m thick. It is based on the NEMO OGCM with a reduced order localized Kalman filter analysis. In situ temperature and salinity from the CORA database are assimilated on a weekly basis together with satellite SST and along track AVISO SLA to constrain the ocean circulation. The atmospheric forcing comes from the ERAi atmospheric reanalysis, with an additional correction applied to the precipitation to be closer to the PMWC observations. Climatological river runoffs are deduced from the Dai and Trenberth database. There is no restoring term to any SSS estimate in the open ocean. The reanalysis outputs were monthly averaged and interpolated on the EASE grid of the ESA CCI SSS for the intercomparison. We also consider the twin simulation to GLORYS12v1 but without any data assimilated to assess the ability of the forced NEMO model configuration to represent the SSS variability at global scale and the impact of data assimilation.

In this study done at the beginning of the project, we used the ESA CCI SSS v03.21 Monthly data with a 25 km spatial resolution. It was the latest version available at that time.

Effect of data assimilation on SSS variability from 2011-2016

The overall correlation between the ESA CCI SSS and the GLORYS12v1 and GLORYS12-free simulations were computed over the common period 2011-2016. Figure 21 shows high correlation values in the open ocean, especially in the tropical band with a significant improvement when observations are assimilated. High latitudes are less correlated with an anti-correlation in the subpolar gyre. In this region, the SSS product has a quite large error.

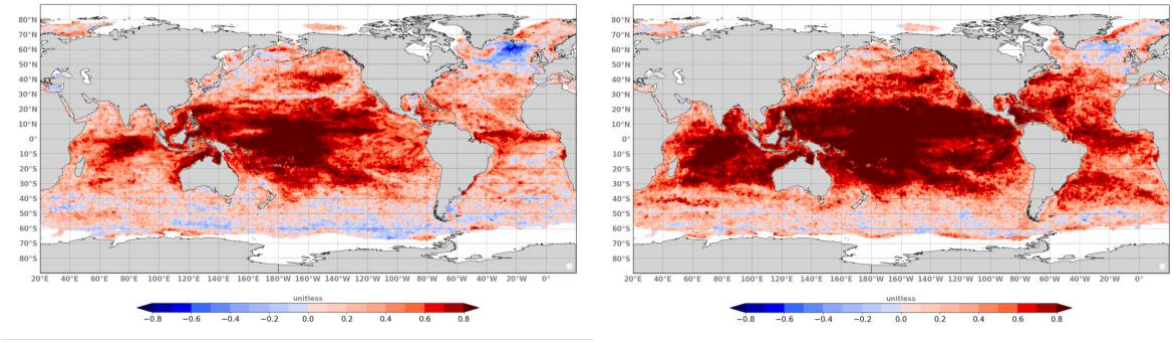

Figure 21 : SSS correlation between ESA CCI SSS v3.21 and Glorys12 « free » (left); Glorys 12 (right) SSS.

Seasonal and interannual variability

An EOF decomposition was conducted to better specify the variability of the SSS at global scale. Figure 22 shows the 1st EOF pattern and time evolution for the ESA CCI SSS and the GLORYS12 SSS from 2011 to 2019. The 2nd EOF variability is also mostly seasonal but with different patterns than the 1st EOF even if still dominated by the tropical ocean variability.

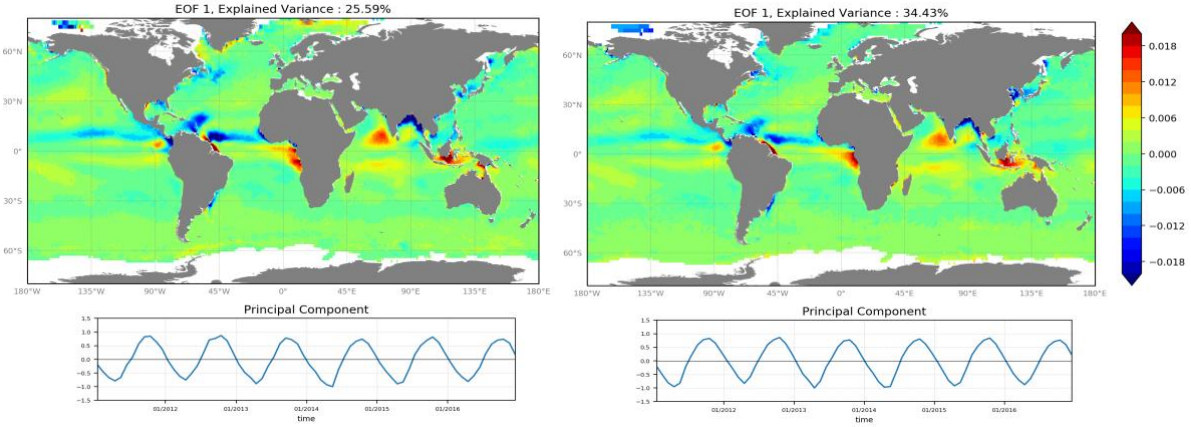

Figure 22: 1st EOF of the SSS decomposition over the period 2011 - 2019 for the ESA CCI (left) and GLORYS12 (right) SSS in PSU.

The seasonal cycle dominates the SSS variability and is driven by river outflows. It explains 40% of the variance in ESA CCI compared to 55% in GLORYS12. This could be due to the absence of river runoff interannual variability. The patterns and time series for this 1st EOF is very similar between the reanalysis and the ESA CCI SSS, it is also the case for the 2nd and 3d EOFs (not shown here).

Then an EOF decomposition was done after removing the seasonal cycle in both time series. The 1st EOF Figure 23 has a pattern linked to ITCZ/SPCZ and river outflows that is very similar between ESA CCI and GLORYS12 SSS. The amplitude of the patterns are slightly higher in the model compared to the satellite SSS, and the Labrador current shows a significant variability in the satellite SSS not seen in the model.

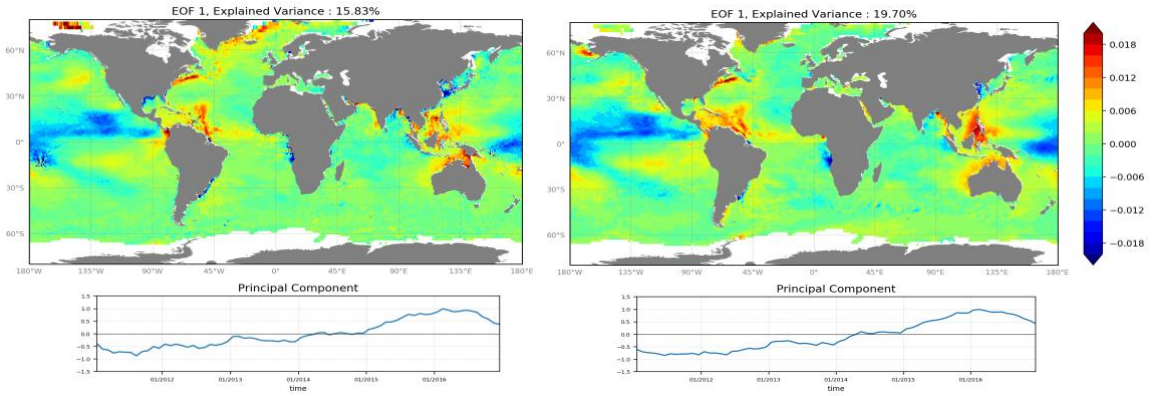

Figure 23: 1st EOF of the SSS when removing the seasonal cycle for the ESA CCI SSS and GLORYS12 SSS between 2011 – 2019.

The analysis shows that GLORYS12 have similar trends and variability when compared to ESA CCI despite the climatological runoff forcing, except in the subpolar gyre.

The Free GLORYS12 simulation strongly differs from ESA SSS and GLORYS12 highlighting the benefit of data assimilation to constrain the SSS in the open ocean at large scale. The tropical oceans are dominating the global ocean variability at seasonal and interannual scales, correlated with the monsoon, then precipitation and linked to ENSO. The satellite SSS products are unique to evaluate the SSS from model outputs, since in situ observations are too sparse to assess the different scales.

Next steps:

A new reanalysis at 1/12° is planned to be produced next year, we will compare the SSS estimates with the ESA CCI product, in its version 4, so the intercomparison will reflect the latest version of both reanalysis and satellite observations. In the meantime, sensitivity analysis to runoff specification will be running with the NEMO model and evaluated against the ESA CCI SSS data.

5 SUMMARY

In this climate assessment report, we have presented seven case studies undertaken to evaluate the quality of CCI+SSS products and their efficiency for climate studies and relevancy for operational operators.

Combined to regional ocean and coupled models, CCI+SSS v3 and v4.4 have shown their relevance to provide a SSS baseline of the Amazon River plume at interannual scale. A cross ECV analysis using CCI+SSS and ocean color products brought insight on the role of dissolved organic matter on the biogeochemical and physical properties of the plume.

The synergy of SSS from satellites measurement (CCI+SSS v4.4 product) and in situ measurements (at lower resolution) have improved the signal-to-noise ratio of SSS in cold SST regions, such as the Artic. The interannual variability of SSS in Barents Sea can be now monitored with a reduced bias and error of the order of 0.5 pss, providing new and more "synoptic" insights into the mechanisms of SSS variability in relation to local freshwater cycle.

Tests have been performed in order to prepare the update of the data assimilation (DA) and forecasting system used at the Met Office for operational ocean and sea-ice forecasting so that it makes use of the latest developments in model and uses updated versions of the satellite SSS datasets, and improves the assimilation of satellite SSS data. This work ended up with a configuration for assimilation of SSS data which gives some improvements to the accuracy of the model's SSS field compared to the previous set-up, while some further improvements could be made, particularly regarding the observation bias correction for the SMOS and SMAP satellite data.

Finally, the CCI+SSS product has proven its relevance for validating interannual variability and multi-year trends in SSS on regional and global scales.

REFERENCES

Barbosa Aguiar, A., Bell, M.J., Blockley, E., Calvert, D., Crocker, R., Inverarity, G., King, R., Lea, D.J., Maksymczuk, J., Martin, M.J., Price, M., Waters, J., While, J., Siddorn, J., Smout-Day, K. The Met Office Forecast Ocean Assimilation Model (FOAM) using a 1/12 degree grid for global forecasts. Submitted to Quarterly Journal of the Royal Meteorological Society.

Blindheim, J. and Rey, F.: Water-mass formation and distribution in the Nordic Seas during the 1990s, J. Mar. Sci., 61, 846–863, 2004.

Boutin J., Vergely J.L., Marchand S., D'Amico F., Hasson A., Kolodziejczyk Nicolas, Reul Nicolas, Reverdin G., Vialard J. (2018). New SMOS Sea Surface Salinity with reduced systematic errors and improved variability. Remote Sensing of Environment, 214, 115-134. http://doi.org/10.1016/j.rse.2018.05.022.

Barichivich, J., Gloor, E., Peylin, P., Brienen, R. J., Schöngart, J., Espinoza, J. C., & Pattnayak, K. C. (2018). Recent intensification of Amazon flooding extremes driven by strengthened Walker circulation. *Science advances*, *4*(9), eaat8785.

Dagg, M., Benner, R., Lohrenz, S., & Lawrence, D. (2004). Transformation of dissolved and particulate materials on continental shelves influenced by large rivers: plume processes. *Continental shelf research*, *24*(7-8), 833-858.

da Cunha, L. C., & Buitenhuis, E. T. (2013). Riverine influence on the tropical Atlantic Ocean biogeochemistry. Biogeosciences, 10(10), 6357-6373.

Del Vecchio, R., & Subramaniam, A. (2004). Influence of the Amazon River on the surface optical properties of the western tropical North Atlantic Ocean. *Journal of Geophysical Research: Oceans*, *109*(C11).

Foltz, G. R., McPhaden, M. J., & Lumpkin, R. (2012). A strong Atlantic meridional mode event in 2009: The role of mixed layer dynamics. Journal of Climate, 25(1), 363-380.

Fournier, S., Chapron, B., Salisbury, J., Vandemark, D., & Reul, N. (2015). Comparison of spaceborne measurements of sea surface salinity and colored detrital matter in the Amazon plume. *Journal of Geophysical Research: Oceans*, *120*(5), 3177-3192.

Garcia-Olivares, A., Isern-Fontanet, J., and Garcia-Ladona, E.: Dispersion of passive tracers and finite-scale Lyapunov exponents in the Western Mediterranean Sea, *Deep-Sea Res. Pt.* I, 54, 253–268, 2007.

Gévaudan, M., Jouanno, J., Durand, F., Morvan, G., Renault, L., & Samson, G. (2021). Influence of ocean salinity stratification on the tropical Atlantic Ocean surface. *Climate Dynamics*, *57*(1-2), 321-340.

Gévaudan, M., Durand, F., & Jouanno, J. (2022). Influence of the Amazon-Orinoco Discharge Interannual Variability on the Western Tropical Atlantic Salinity and Temperature. *Journal of Geophysical Research: Oceans*, *127*(6), e2022JC018495.

Gévaudan, M., Jouanno, J., Aumont, O., Boutin, J. (in prep). On the importance of riverine organic matter for the Amazon plume productivity. *In prep for Geophysical Research Letters*

Holliday, N. P., Bersch, M., Berx, B., Chafik, L., Cunningham, S., Florindo-López, C., Hátún, H., Johns, W., Josey, S. A., Larsen, K. M. H., Mulet, S., Oltmanns, M., Reverdin, G., Rossby, T., Thierry, V., Valdimarsson, H., and Yashayaev, I.: Ocean circulation causes the largest freshening event for 129 years in eastern dubpolar North Atlantic. Nat. Commun., 11, 585, 2020

Holst, J. C., Røttingen, I., and Melle, W.: The herring, in: The Norwegian Sea Ecosystem, edited by: Skjoldal, H. R., Tapir Aca- demic Press, Trondheim, Norway, 203–226, 2004.

Lin, W., Portabella, M., Stoffelen, A., Turiel, A., and Verhoef, A.: Rain identification in ASCAT winds using singularity analysis, IEEE Geosci. Remote Sens. Lett., 11, 1519–1523, https://doi.org/10.1109/LGRS.2014.2298095, 2014.

Louchard, D., Gruber, N., & Münnich, M. (2021). The impact of the Amazon on the biological pump and the air-sea CO2 balance of the Western Tropical Atlantic. Global Biogeochemical Cycles, 35(6), e2020GB006818.

Martin, M. J., E. Remy, B. Tranchant, R. R. King, E. Greiner & C. Donlon (2020). Observation impact statement on satellite sea surface salinity data from two operational global ocean forecasting systems, Journal of Operational Oceanography, DOI: 10.1080/1755876X.2020.1771815.

Martin M.J., King R.R., While J., Aguiar A.B. Assimilating satellite sea-surface salinity data from SMOS, Aquarius and SMAP into a global ocean forecasting system. Q J R Meteorol Soc 2019;145:705–726. https://doi.org/10.1002/qj.3461

Meissner, T., F. J. Wentz, A. Manaster, R. Lindsley, M. Brewer, M. Densberger, 2022: Remote Sensing Systems SMAP Ocean Surface Salinities [Level 2C], Version 5.0 validated release. Remote Sensing Systems, Santa Rosa, CA, USA. Available online at www.remss.com/missions/smap, doi: 10.5067/SMP50-2SOCS

Melle, W., Ellertsen, B., and Skjoldal, H. R.: Zooplankton: The link to higher trophic levels, in: the Norwegian Sea Ecosystem, 137– 202, Tapir Academic Press, Trondheim, 2004.

Mork, K. A., Skagseth, Ø., and Søiland, H.: Recent warming and freshening of the Norwegian Sea observed by Argo data. J. Clim., 32, 3695-3705, 2019

Olivier, L., Reverdin, G., Boutin, J., Laxenaire, R., Iudicone, D., Pesant, S., Calil, P., Horstmann, J., Couet, D., Erta, J. M., Koch-Larrouy, A., Bertrand, A., Rousselot, P., Vergely, J.-L., Speich S., and Araujo, M. Late summer northwestward Amazon plume pathway under the action of the North Brazil Current rings. Submitted to Rem. Sens Res.

Oke, P. R., and P. Sakov, 2008: Representation Error of Oceanic Observations for Data Assimilation. J. Atmos. Oceanic Technol., 25, 1004–1017, https://doi.org/10.1175/2007JTECHO558.1.

Ozhigin, V. K., and Ivshin, V. A.: Water masses of the Barents Sea. PINRO Press. In Russian. Murmansk, Russia, 48pp, 1999

Portabella, M., Stoffelen, A., Lin, W., Turiel, A., Verhoef, A., Verspeek, J., and Ballabrera-Poy, J.: Rain effects on ASCAT retrieved winds: towards an improved quality con- trol, IEEE Geosci. Remote Sens. Lett., 50, 2495–2506, https://doi.org/10.1109/TGRS.2012.2185933, 2012.

Reverdin, G., Olivier, L., Cabanes, C., Boutin, J., Thouvenin-Masson, C., Vergely, J.-L., Kolodziejczyk, N., Thierry, V., Khvorostyanov, D., and Jouanno, J. (2023). Are Argo floats profiling in the Amazon river plume? J.Atmos. Oceanogr. Tech.

Rudels, B., Jones, E. P., Schauer, U., and Eriksson, P.: Atlantic sources of the Arctic Ocean surface and halocline waters. Polar Res., 23(2), 181-208, 2004

Rudels, B., Muench, R. D., Gunn, J., Schauer, U., and Friedrich, H. J.: Evolution of the Arctic boundary current north of the Siberian shelves. J. Mar. Sys., 25, 77-99, 2000

Schauer, U., Loeng, H., Rudels, B., Ozhigin, V. K., and Dieck, W.: Atlantic water inflow through the Barents and Kara Seas. Deep-Sea Res. Part I, 49, 2281-2298, 2002

Subramaniam, A., Yager, P. L., Carpenter, E. J., Mahaffey, C., Björkman, K., Cooley, S., ... & Capone, D. G. (2008). Amazon River enhances diazotrophy and carbon sequestration in the tropical North Atlantic Ocean. Proceedings of the National Academy of Sciences, 105(30), 10460-10465.

Turiel, A., Nieves, V., Garcia-Ladona, E., Font, J., Rio, M.-H., and Larnicol, G.: The multifractal structure of satellite sea surface temperature maps can be used to obtain global maps of stream-lines, Ocean Sci., 5, 447–460, https://doi.org/10.5194/os-5-447- 2009, 2009.

End of document